ACS OMEGA

http://pubs.acs.org/journal/acsodf

Article

Computational Exploration of Anti-cancer Potential of Flavonoids against Cyclin-Dependent Kinase 8: An *In Silico* Molecular Docking and Dynamic Approach

Sanket Rathod,* Ketaki Shinde, Jaykedar Porlekar, Prafulla Choudhari, Rakesh Dhavale, Deepak Mahuli, Yasinalli Tamboli, Manish Bhatia, Kishan P. Haval, Abdullah G. Al-Sehemi, and Mehboobali Pannipara

Cite This: *ACS Omega* 2023, 8, 391−409

Read Online

ACCESS | Metrics & More | Article Recommendations | Supporting Information

ABSTRACT: Over the centuries, cancer has been considered one of the significant health threats. It holds the position in the list of deadliest diseases over the globe. In women, breast cancer is the most common among many cancers and is the second most common cancer all over the world, while lung cancer is the first. Cyclin-dependent kinase 8 (CDK8) has been identified as a critical oncogenic driver that is found in breast cancer and associated with tumor progression. Flavonoids were virtually screened against CDK8 using molecular docking, drug-likeness, ADMET prediction, and a molecular dynamics (MD) simulation approach to determine the potential flavonoid structure against CDK8. The results indicated that ZINC000005854718 showed the highest negative binding affinity of −10.7 kcal/mol with the targeted protein and passed all the drug-likeness parameters. Performed molecular dynamics simulation showed that docked complex systems have good conformational stability over 100 ns in different temperatures (298, 300, 305, 310, and 320 K). The comparison between calculated binding free energy *via* MM/PB(GB)SA methods and binding affinity calculated *via* molecular docking suggested tight binding of ZINC000005854718 with targeted protein. The results concluded that ZINC000005854718 has drug-like properties with tight and stable binding with the targeted protein.

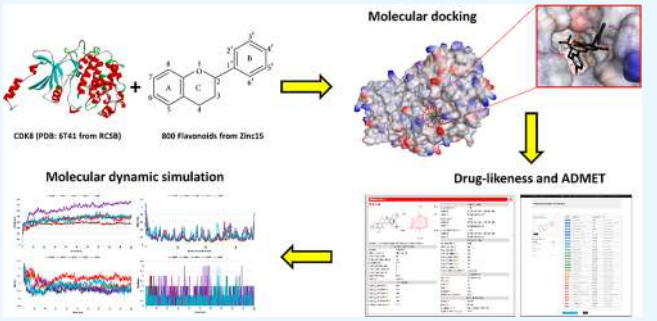

1. INTRODUCTION

Cancer is the primary cause of mortality worldwide and the second leading cause of death.[1] More than 277 different types of cancers have been discovered by scientists.[2] Prostate, lung, bronchus, colon, rectum, and urinary bladder cancers are commonly seen in men, while breast, lung, bronchus, colon, rectum, uterine corpus, and thyroid cancers are common in women.[3−5] Prostate and breast cancer cases are widely reported as compared to other cancers.[2,3,6] Public health issues related to breast cancer are getting worse. Significant progress has been achieved in treating breast cancer, but it has been less successful in predicting high-risk women and preventing the disease.[7] Breast cancer has had the greatest cancer incidence in women worldwide for a long time. Parent-inherited genetic variants are responsible for 5−10% of breast tumors. Women with close blood relatives are at higher risk for breast cancer, even though less than 15% of breast cancer patients have a family history of the concerned disease. For instance, a woman's risk of developing breast cancer gets doubled if her mother, sister, or daughter has the condition, and it gets roughly tripled if two of her first-degree relatives have it.[8] Hormones frequently used in birth control methods may increase the risk of breast cancer. Depo-Provera, an injectable form of progesterone, has been linked to an increased risk of breast cancer, although this does not appear to be the case 5 years after the doses are stopped.[9] In the current era, screening mammography detects more than half of breast cancer cases in the United States, with around one-third diagnosed as palpable breast tumors.[10]

Aberrant cell proliferation and irregular gene functioning are hallmarks of any type of cancer. In human cells, cyclin-dependent kinases (CDKs) help to control the critical cell cycle and transcription events that lead to proliferation.[11,12] In various proliferative diseases such as cancer, CDK acts as a small part of serine/threonine protein kinases, which may be a potential therapeutic target.[13] The CDK family is classified into three types: the first cell cycle-related subfamilies include CDK1, CDK4, and CDK5; the second transcriptional subfamilies include CDK7, cyclin-dependent kinase 8 (CDK8), CDK9, CDK11, and CDK20; and others may

Received: July 30, 2022
Accepted: December 9, 2022
Published: December 21, 2022

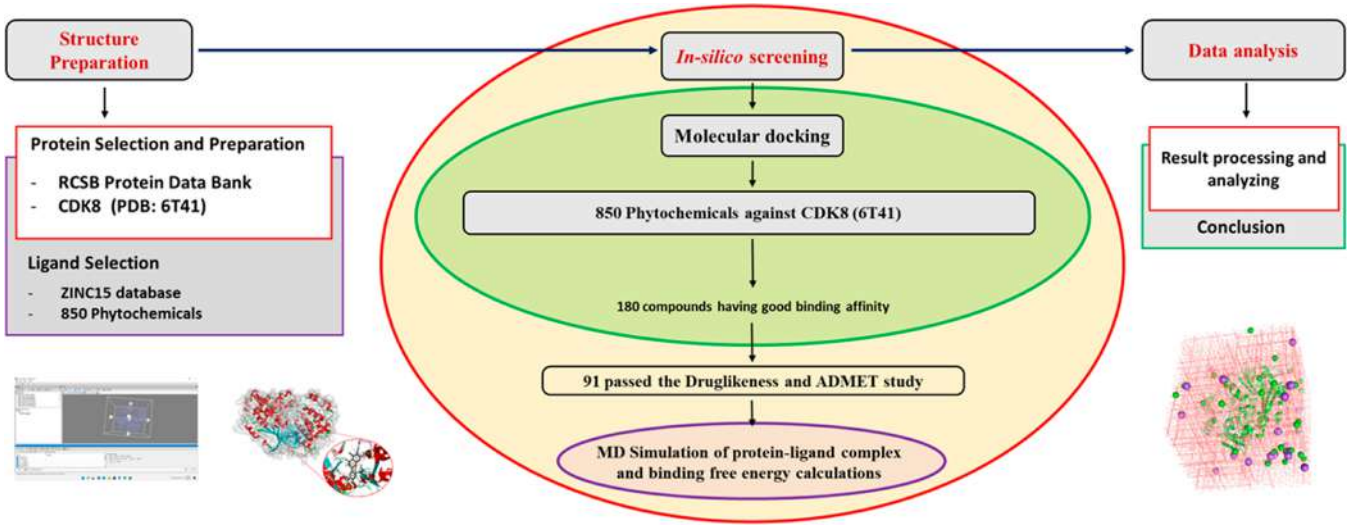

Figure 1. Schematic representation of workflow applied in the current research.

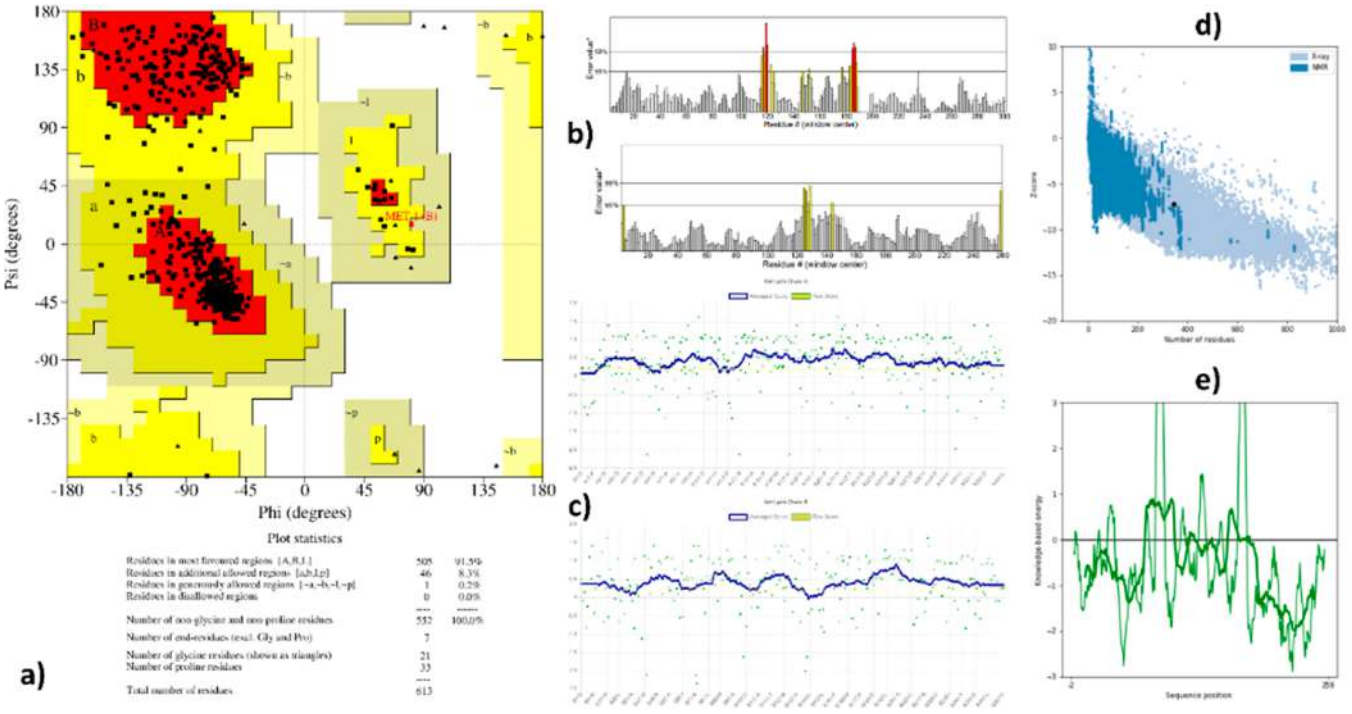

Figure 2. Validation and quality evaluation of the prepared protein structure (PDB: 6T41) by using (a) Ramachandran plot (PROCHECK), (b) ERRAT, and (c) Verify3D plot showing amino acids in favored regions. (d) Overall model quality and (e) local model quality observed *via* ProSA-web.

contain CDK5, CDK14−18, and so forth.[14] CDKs are one of the primary regulators of the cell cycle and transcription.[15] Specifically, CDK8 plays a crucial role in transcription and oncogenesis, which is known to be a large transcription member of the CDK family and has received special attention for research. CDK8 has been identified as a key driver of oncogenesis in many cancers.[16] The enzyme CDK8 controls the transcription by either interacting with the mediator complex or by phosphorylating the transcription factors.[17] Factors which contributes to oncogenesis in case of colorectal, breast and hematological cancer include activation by CDK8, Wnt/β-catenin signaling, transcription associated with estrogen inducible genes and depriving levels of super-enhancer associated genes.[18] CDK8 may act as a multiprotein which manages the RNA polymerase II-dependent transcription. Most research has already been done and reported the role of CDK8s as an oncogene. The various biological functions of CDK8 and its allegedly context-specific significance in many types of cancers have inspired considerable interest, and maybe even more disagreement, in developing CDK8 inhibitors as prospective cancer therapy agents.[16] Flavonoids are plant-based phenolic compounds having metabolism process modulatory activity to prevent degenerative and chronic diseases.[19,20] Flavonoids are an essential class of plant-based secondary metabolites.[21] Flavonoid compounds have a broad range of therapeutic activities such as anti-cancer activity, anti-viral/bacterial activity, anti-inflammatory activity, anti-age-dependent neuropathology activity, anti-diabetic activity,

https://doi.org/10.1021/acsomega.2c04837
ACS Omega 2023, 8, 391−409

cardioprotective activity, and anti-oxidant activity.[21−27] In the current work, number of phytochemicals were used to screen against CDK8.

Identification of drug candidates *via* a computational screening approach is a promising and cost-effective strategy that plays a vital role in the drug discovery and development pipeline.[28] Computational chemistry based approaches in target identification and drug discovery help medicinal chemists cover the broad range of theoretical parts of modern drug discovery.[29] Nowadays, computational tools are getting more and more advanced, and it is made possible due to the increased capabilities of computers, supercomputers, and parallel computing techniques to handle critical tasks of the drug discovery pipeline.[30] In the present study, molecular docking study, drug-likeness prediction, ADMET prediction, molecular dynamics (MD) simulation study, and binding free energy calculations were applied to identify potential lead candidates from screened ligand library. Molecular docking was done to find the potential flavonoids having a good binding affinity with CDK8 (PDB: 6T41). The drug-likeness and ADMET prediction were made to identify the drug-like compound. Pharmacophore modeling was done to explore the standard pharmacophoric features in docked compounds. A MD simulation study provides real-time confirmation of the stability of the protein−ligand complex over the simulated time scale. Computer-aided drug discovery (CADD) reduces the time and cost of experimental work.[31,32] A schematic representation of different computational studies applied in the current work is illustrated in Figure 1.

2. RESULTS

2.1. Protein and Ligand Preparation. The prepared protein structure of PDB: 6T41 was subjected to quality evaluation using various online tools. Ramachandran plot for PDB: 6T41 was generated using the PROCHECK server and studied to determine the changes that occurred in the protein structure after the protein preparation process. The generated Ramachandran plot revealed that 91.5% of residues are present in favored regions, as shown in Figure 2a. The overall quality factor obtained from ERRAT for the prepared protein structures was found to be 96.1149% (Figure 2b). Verify3D score results indicated that 91.52% of the amino acid residues are averaged the atomic model (3D) to amino acid sequence (1D) score ≥0.2, which is a good score (Figure 2c). The z-scores obtained from the ProSA-web server for all chains in PDB: 6T41 are determined by X-ray crystallography (light blue) or NMR spectroscopy (dark blue) regarding their length, and the overall model quality as the z-score of PDB: 6T41 is −7.22, which is highlighted in Figure 2d with a black dot. Figure 2e represents the local model quality obtained from ProSA-web energy plot of PDB: 6T41 in which the thick line indicates the average energy throughout each 40-residue fragment while a thin line in the plot's background indicates average energy with a window size of 10 residues. Binding pocket analysis using BIOVIA Discovery Studio revealed that VAL27, GLY28, TYR32, VAL35, TYR36, LYS37, ALA38, ASP48, TYR49, ALA50, LEU51, LYS52, PHE97, ASP98, TYR99, ALA100, GLU101, HIS102, ASP103, LEU104, TRP105, HIS106, PRO154, ALA155, ASN156, ILE157, LEU158, VAL159, MET160, GLY161, ARG168, VAL169, LYS170, ILE171, ALA172, ASP173, MET174, and ARG356 are the key amino acid residues present in the analyzed binding pocket of PDB: 6T41, and the identified binding pocket is represented with the yellow sphere in Figure 3. Ligands were energy-minimized using the OpenBabel package of PyRx and used for further *in silico* studies.

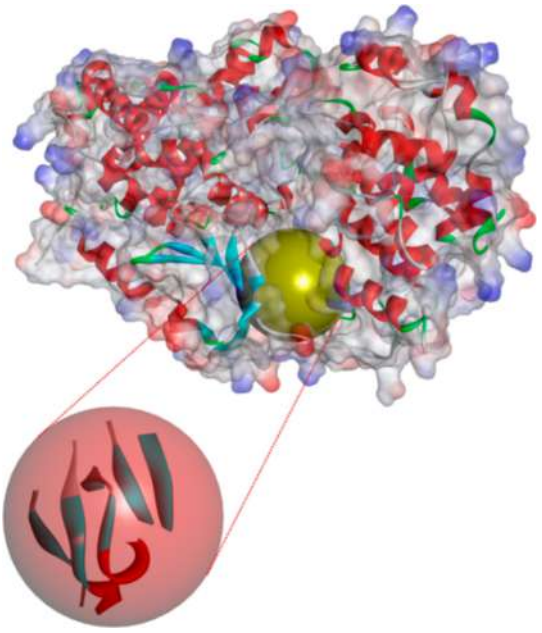

Figure 3. Highlighted yellow sphere represents the identified binding pocket in PDB: 6T41.

2.2. Molecular Docking. A molecular docking study was carried out using flavonoid structures as ligand groups and CDK8 as a macromolecule. The AutoDock Vina program of PyRx 0.8 was used to perform the molecular docking study.[33,34] Downloaded structures of flavonoids and standards were docked against CDK8 using the algorithm of docking software to obtain the binding confirmations and binding affinity. Eight hundred structures of flavonoids along with five standards {*N*-[(4-chlorophenyl)methyl]quinazolin-4-amine, CCT251545, ponatinib, linifanib, and cortistatin A} were docked, and the binding affinity of flavonoids and standards were compared. The results of the molecular docking study showed that out of all the docked flavonoids, ZINC000005854718 showed a binding affinity of −10.7 kcal/mol with CDK8 (PDB: 6T41). The resulting binding affinity of standards obtained *via* molecular docking was found as **STD1** {*N*-[(4-chlorophenyl)methyl]quinazolin-4-amine} showed a binding affinity of −8.6 kcal/mol, **STD2** (CCT251545) showed a binding affinity of −8.1 kcal/mol, **STD3** (ponatinib) showed a binding affinity of −10 kcal/mol, **STD4** (linifanib) showed a binding affinity of −10.5 kcal/mol, and **STD5** (cortistatin A) showed a binding affinity of −10.1 kcal/mol. The binding affinity of ZINC000005854718 and ZINC000013485410 was found to be the lowest as compared to the used standards. The visualized interactions of ligands in the binding pocket of PDB: 6T41 indicated that all the docked ligands are bound in the obtained binding pocket (Figure 3). Binding interactions indicated that the GLY28 residue is involved to form a carbon−hydrogen bond (HB) between the targeted protein and all the docked ligands. Figure 4a,b represents the 3D visual of ZINC000005854718 binding in the binding pocket of PDB: 6T41. Figure 4c indicates the representation of 2D binding interactions of ZINC000005854718 with PDB: 6T41, showing that the ligand

https://doi.org/10.1021/acsomega.2c04837
ACS Omega 2023, 8, 391−409

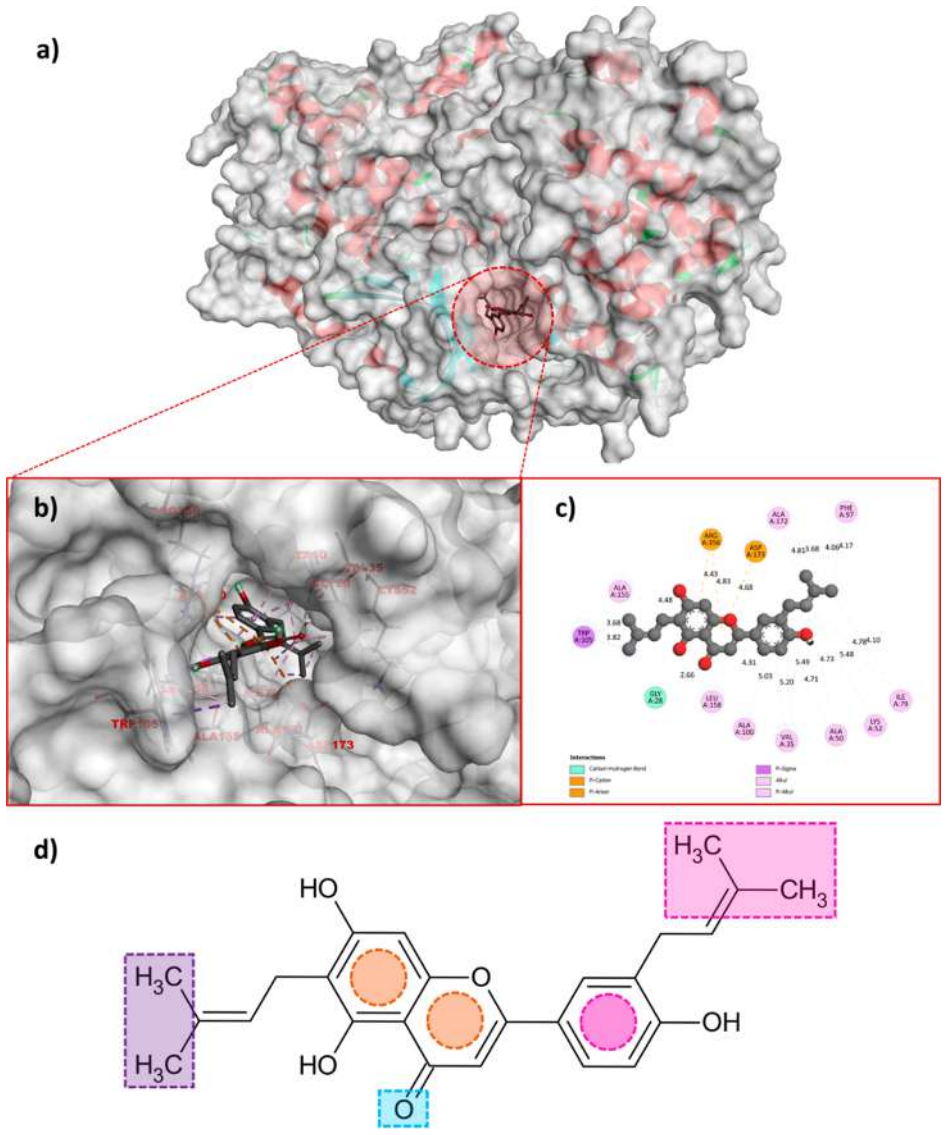

Figure 4. (a) ZINC000005854718 bound in the binding cavity of 6T41, (b) 3D view of ligand binding in the binding cavity and (c) 2D interaction of ZINC000005854718 with 6T41, and (d) highlighted interacting groups of ZINC000005854718.

group was formed by binding with GLY28, ARG356, ASP173, TRP105, LEU158, VAL35, LYS52, PHE97, ALA50, ALA155, ALA100, ALA172, ILE79, and all these amino acid residues are present in the active pocket obtained *via* binding pocket analysis. In Figure 4d, the interacting groups of ZINC000005854718 are highlighted with respective colors. CH_3 groups highlighted with the purple colored box indicate the $\pi-\sigma$ interaction with TRP105. The ARG356 and ASP173 amino acid residues of the targeted protein are involved in $\pi-$cations and $\pi-$anions with the aromatic rings present in ZINC000005854718 and highlighted with orange circles in Figure 4d. The highlighted oxygen group with sky blue color formed a carbon−HB (covalent bond) with GLY28, and all the CH_3 groups highlighted with pink color formed alkyl and $\pi-$alkyl interactions with LEU158, VAL35, LYS52, PHE97, ALA50, ALA155, ALA100, ALA172, and ILE79. The covalent binding between the oxygen group and GLY28 showed the lowest distance (2.66 Å), and this interaction may contribute to the formation of the stable protein−ligand complex. The 3D visualization indicating the ligand interactions with the targeted protein is represented in Figure 5. Through the results of molecular docking, it is found that 180 out of 800 docked flavonoids have a binding affinity of more than −9 kcal/mol with CDK8 (PDB: 6T41). The ligands having a binding affinity of more than −9 kcal/mol were further subjected to drug-likeness prediction. The interactions of top-docked flavonoids with a binding affinity of more than −9 kcal/mol are represented in Table S1. The interactions of the first 10 flavonoids with the highest negative binding affinity and docked standards are represented in Table 1. The protein−ligand complex of 6T41−ZINC000005854718 was further subjected to a MD simulation study to determine the stability of the complex system.

2.3. Drug-Likeness and *In Silico* ADMET. Drug-likeness and *in silico* ADMET profiling are necessary tasks in the drug discovery pipeline because it gives information regarding the drug-like properties of the ligand structure. A compound is denoted as a drug candidate only if it passes the drug-likeness prediction. Lipinski's rule of five is a commonly applied rule to determine the drug-like properties of compounds. Rule of five is a set of phytochemical parameters including molecular weight (MW), lipophilicity (mLog *P*), number of HB

https://doi.org/10.1021/acsomega.2c04837
ACS Omega 2023, 8, 391−409

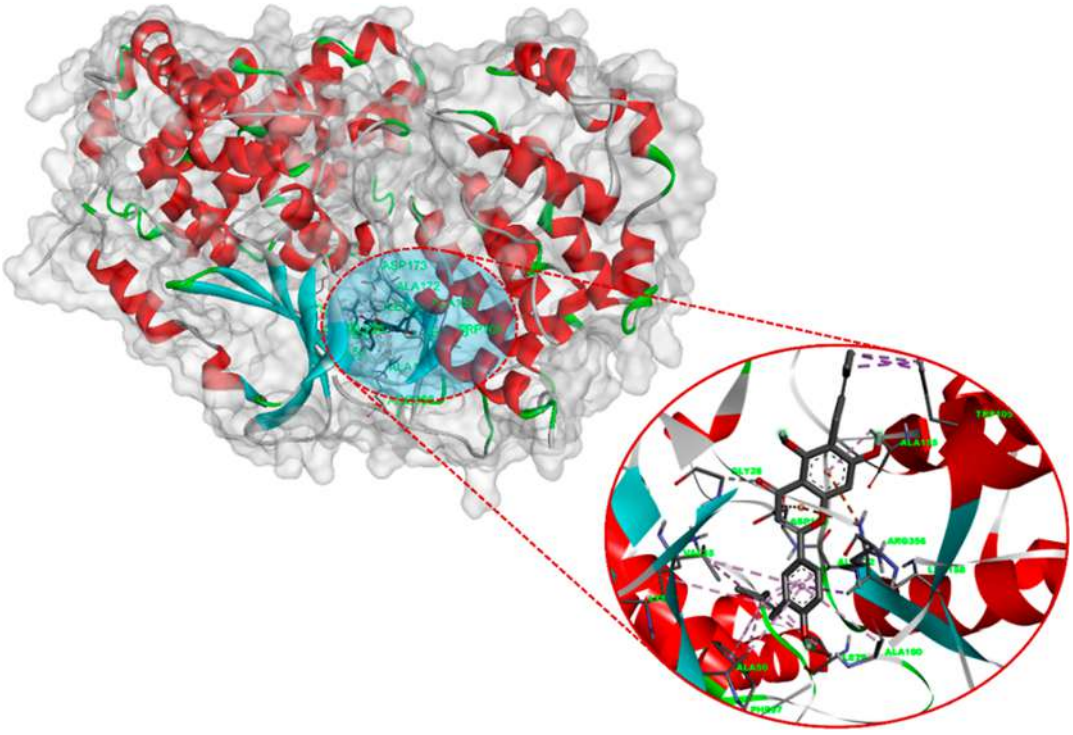

Figure 5. 3D representation of protein−ligand interactions.

acceptors (nHBA), number of hydrogen bond donors (nHBD), and molar refractivity (MR). After molecular docking, it is found that a total of 180 flavonoids showed a binding affinity of more than −9 kcal/mol, and these 180 flavonoids were subjected to drug-likeness prediction using SwissADME, and through the results, it is observed that 91 out of 180 flavonoids followed Lipinski's rule of five with a minimum or zero violation in the rule. Along with Lipinski's rule of five, other physicochemical properties such as the topological polar surface area (TPSA) and the number of rotatable bonds (nRot) were determined using SwissADME, and 91 flavonoids were passed all these properties. Medicinal chemistry (PAINS #alerts and Brenk #alerts) of structures was also predicted using SwissADME. The results of drug-likeness prediction of all 91 flavonoids with a binding affinity of more than −9 kcal/mol are represented in Table S2, and out of 91 flavonoids, the first 10 flavonoids with the highest negative binding affinity are represented in Table 2. Pharmacokinetics (ADMET) profiling of 91 flavonoid structures having good drug-likeness properties was determined using pkCSM servers. Through the results of ADMET prediction, it is observed that almost all the selected flavonoids have good ADMET properties, as shown in Tables 3 and S3. Four out of 91 flavonoids showed positive results in AMES toxicity, and hence, they may not be mutagenic in nature. Drug-likeness and *in silico* ADMET profiling of ZINC000005854718, which showed the highest negative binding affinity *via* molecular docking, showed satisfactory results with good drug-like properties and it also followed the ADMET requirements.

2.4. MD Simulation. 6T41−ZINC000005854718 showed the highest negative binding affinity and followed all the parameters to be a drug-like candidate. Hence, the MD simulation study using this protein−ligand complex along with the empty targeted CDK8 structure (PDB: 6T41) was performed. The estimation and comparison of the stability, conformational changes, and residual fluctuations in the complexes and empty protein over the 100 ns simulation were done using a simulated MD trajectory. The MD simulation study of the targeted CDK8 structure (PDB: 6T41) in the varied temperature condition resulted in increased fluctuations in the root-mean-square fluctuations (RMSFs) as shown in Figure S1. The CDK8 structure responded differently in all the simulated temperatures. The structure of CDK8 (PDB: 6T41) attained the minimum residual fluctuations in 305 and 320 K as compared to the other temperatures. In the body temperature (310 K), the structure of CDK8 (PDB: 6T41) showed increased RMSFs ranging from ∼0.5 to ∼3 nm. Similarly, the structure of CDK8 (PDB: 6T41) showed increased RMSFs at room temperature (298−300 K). The selected protein−ligand complex (6T41−ZINC000005854718) was also simulated in five different temperature conditions to determine its configurational changes that occurred in 298, 300, 305, 310, and 320 K. The root-mean-square deviations (RMSDs), RMSFs, radius of gyration (R_g), HB analysis, and principal component analysis (PCA) were carried out using the final MD trajectories.

The RMSD profiling of the simulated complex was carried out to determine the dynamic behavior and stability over the course of 100 ns. Through the RMSD analysis, it is observed that the 6T41−ZINC000005854718 complex showed the highest stable confirmations with minimum deviations in 298 K with RMSD ranging from ∼0.3 to 0.4 nm. The calculated RMSD of the complex simulated at 300 K ranged between ∼0.3 and ∼0.5 nm, and the RMSD of 6T41−ZINC000005854718 simulated in the body temperature (310 K) indicated increased scattering in the RMSD plot (ranging from 0.4 to 0.8 nm) as compared to the other four temperature conditions. The calculated RMSD for simulation at 320 K indicated the minimum scattering in RMSD values. The RMSD plots analyzed for 6T41−ZINC000005854718 at

https://doi.org/10.1021/acsomega.2c04837
ACS Omega 2023, 8, 391−409

Table 1. Binding Affinity of Flavonoids against CDK8 (PDB: 6T41) along with the Interacting Residue and the Type of Interaction

compound ID	binding affinity (kcal/mol)	interacting residues	distance	type of interaction
N-[(4-chlorophenyl)methyl]quinazolin-4-amine (**STD1**)	−8.6	ARG356	4.78	π−cation
		PHE97	3.92	π−π stacked
		VAL35	3.81, 4.28	π−alkyl
		ALA50	4.91	π−alkyl
		VAL27	5.31	π−alkyl
		ALA172	4.52	π−alkyl
		LYS52	4.96	π−alkyl
		ILE79	4.86	π−alkyl
		PHE97	5.02	π−alkyl
4TV (CCT251545) (**STD2**)	−8.1	SER221	3.59	carbon HB
		ALA2	3.16	carbon HB
		ARG157	3.38	carbon HB
		PHE195	4.14	π−π stacked
		PRO194	4.97	π−alkyl
		PRO158	4.06	π−alkyl
ponatinib (**STD3**)	−10	ARG356	2.93	carbon HB
		ASP173	3.46	carbon HB
		TRP105	3.95	π−σ
		ALA100	3.26	halogen (fluorine)
		TRP105	4.73, 5.09, 6.11	π−π stacked, π−π T shaped
		HIS106	4.89	π−π stacked
		VAL27	5.17	alkyl, π−alkyl
		VAL35	4.74, 7.79	alkyl, π−alkyl
		LYS153	4.66	alkyl, π−alkyl
		ALA155	4.81, 5.44, 4.90	alkyl, π−alkyl
linifanib (**STD4**)	−10.5	ASP98	2.51	conventional HB
		VAL27	2.27, 2.63	conventional HB
		ALA100	2.50, 2.78	conventional HB
		TYR99	2.97	carbon HB
		TRP105	4.17	π−σ
		HIS106	4.67	π−π stacked, π−π T shaped
		TRP105	6.53	π−π stacked, π−π T shaped
		ALA50	3.55, 4.57	π−alkyl
		LEU158	4.85, 5.05	π−alkyl
		ILE79	5.25, 5.20	π−alkyl
		ALA172	4.62	π−alkyl
		VAL35	5.18, 4.58	π−alkyl
		ALA100	4.59	π−alkyl
cortistatin A (**STD5**)	−10.1	VAL35	4.20, 5.22	alkyl, π−alkyl
		ALA50	3.62, 4.96	alkyl, π−alkyl
		ILE79	5.38	alkyl, π−alkyl
		ALA100	4.95	alkyl, π−alkyl
		LEU158	4.85, 5.10	alkyl, π−alkyl
ZINC000005854718	−10.7	GLY28	2.66	carbon HB
		ARG356	4.43, 4.83	π−cation
		ASP173	4.68	π−anion
		TRP105	3.68, 3.82	π−σ
		LEU158	4.31	alkyl, π−alkyl
		VAL35	5.20, 5.49	alkyl, π−alkyl
		LYS52	5.48	alkyl, π−alkyl
		PHE97	4.06, 4.17	alkyl, π−alkyl
		ALA50	4.71, 4.73	alkyl, π−alkyl
		ALA155	4.48	alkyl, π−alkyl
		ALA100	5.03	alkyl, π−alkyl
		ALA172	4.81, 3.68	alkyl, π−alkyl
		ILE79	4.10, 4.78	alkyl, π−alkyl
ZINC000013485410	−10.6	ASP98	2.54	conventional HB
		GLY28	2.85	carbon HB
		ASP173	4.99	π−anion
		TRP105	3.53, 3.67	π−σ

https://doi.org/10.1021/acsomega.2c04837
ACS Omega 2023, 8, 391−409

Table 1. continued

compound ID	binding affinity (kcal/mol)	interacting residues	distance	type of interaction
		LEU158	4.51	alkyl, π−alkyl
		VAL35	5.13, 5.24	alkyl, π−alkyl
		TRP105	4.94	alkyl, π−alkyl
		ILE79	4.84, 4.25	alkyl, π−alkyl
		ALA50	4.26, 4.86	alkyl, π−alkyl
		LYS52	5.31	alkyl, π−alkyl
		PHE97	4.01, 4.52	alkyl, π−alkyl
		ALA155	4.01, 4.77	alkyl, π−alkyl
		A LA100	4.84	alkyl, π−alkyl
		ALA172	4.82, 3.44	alkyl, π−alkyl
ZINC000005195832	−10.4	ARG29	2.43	conventional HB
		ASP98	2.90	conventional HB
		ASP173	5.00	π−anion
		LEU158	4.50	alkyl, π−alkyl
		VAL35	4.77, 5.10	alkyl, π−alkyl
		LYS52	5.42	alkyl, π−alkyl
		ALA50	4.45, 4.81	alkyl, π−alkyl
		ILE79	4.26, 4.76	alkyl, π−alkyl
		PHE97	4.00, 4.26	alkyl, π−alkyl
		ALA100	5.03	alkyl, π−alkyl
		ALA172	3.72, 4.79	alkyl, π−alkyl
ZINC000002097716	−10.3	ALA100	2.56, 2.75	conventional HB
		ARG356	4.92	conventional HB
		GLY28	2.80	carbon HB
		ASP173	4.02	π−anion
		TRP105	3.59, 3.66	π−σ
		LEU158	4.96	alkyl, π−alkyl
		PHE97	4.02	π−π stacked
		VAL27	5.47	alkyl, π−alkyl
		TRP105	4.48	alkyl, π−alkyl
		VAL35	4.50, 4.21	alkyl, π−alkyl
		LYS52	5.12	alkyl, π−alkyl
		ALA50	4.43	alkyl, π−alkyl
		ILE79	4.77	alkyl, π−alkyl
		ALA155	4.33	alkyl, π−alkyl
		ALA172	4.31	alkyl, π−alkyl
ZINC000013860547	−10.1	ASP98	2.31	conventional HB
		ALA100	2.49	conventional HB
		VAL35	5.26	alkyl, π−alkyl
		ALA100	4.91	alkyl, π−alkyl
		LEU158	5.37, 4.46	alkyl, π−alkyl
		ALA50	4.30, 4.51	alkyl, π−alkyl
		LYS52	5.31	alkyl, π−alkyl
		ILE79	5.00	alkyl, π−alkyl
		PHE97	4.04	alkyl, π−alkyl
		ALA155	4.30	alkyl, π−alkyl
		ALA172	5.09	alkyl, π−alkyl
ZINC000020426551	−10	TYR32	3.00	conventional HB
		ALA100	2.62	conventional HB
		ASN156	2.14	conventional HB
		ASP173	2.53	conventional HB
		ARG356	2.71	conventional HB
		ASP173	3.96	π−anion
		PHE97	3.99, 5.97	π−π stacked
		ILE79	4.84	alkyl, π−alkyl
		VAL35	4.94, 4.49	alkyl, π−alkyl
		LEU158	5.25, 4.93	alkyl, π−alkyl
		ALA50	4.06, 4.69	alkyl, π−alkyl
		LYS52	5.07	alkyl, π−alkyl
		ALA172	4.40	alkyl, π−alkyl
ZINC000012296886	−9.9	TYR32	2.36	conventional HB

https://doi.org/10.1021/acsomega.2c04837
ACS Omega 2023, 8, 391−409

Table 1. continued

compound ID	binding affinity (kcal/mol)	interacting residues	distance	type of interaction
		ALA100	2.34, 2.43	conventional HB
		ASN156	2.84	conventional HB
		ASP173	1.97	conventional HB
		ARG356	2.71, 2.84	conventional HB
		ASP173	4.09	π−anion
		PHE97	3.94	π−π stacked
		ILE79	4.72	alkyl, π−alkyl
		VAL35	4.47, 4.14	alkyl, π−alkyl
		LYS52	5.13	alkyl, π−alkyl
		ALA50	4.05, 5.24	alkyl, π−alkyl
		ALA172	4.35	alkyl, π−alkyl
		LEU158	5.19	alkyl, π−alkyl
ZINC000020763042	−9.9	VAL27	2.34	conventional HB
		ALA100	2.28, 2.47	conventional HB
		ARG356	2.18, 2.37	conventional HB
		GLY28	2.75	carbon HB
		HIS106	2.95	carbon HB
		ASP713	3.99	π−anion
		LEU158	5.04	alkyl, π−alkyl
		PHE97	4.07	π−π stacked
		ALA50	4.32, 5.46	alkyl, π−alkyl
		VAL27	5.35	alkyl, π−alkyl
		LYS52	5.12	alkyl, π−alkyl
		VAL35	4.44, 4.12	alkyl, π−alkyl
		ILE79	4.80	alkyl, π−alkyl
		TRP105	5.34	alkyl, π−alkyl
		HIS106	4.57	alkyl, π−alkyl
		ALA172	4.30	alkyl, π−alkyl
		LEU359	5.34	alkyl, π−alkyl
ZINC000005831326	−9.8	ALA100	2.41, 2.51	conventional HB
		ARG356	2.56	conventional HB
		ARG356	4.69	π−cation
		ASP173	3.96	π−anion
		TYR99	3.01	π−donor H bond
		TRP105	3.71, 3.99	π−σ
		PHE97	4.00	π−π stacked
		VAL35	4.92, 4.46	alkyl, π−alkyl
		TRP105	4.70	alkyl, π−alkyl
		LEU158	5.24, 4.27	alkyl, π−alkyl
		ILE79	4.87	alkyl, π−alkyl
		LYS52	5.02	alkyl, π−alkyl
		ALA172	4.42, 5.18	alkyl, π−alkyl
		ALA50	4.28, 5.02	alkyl, π−alkyl
		ALA155	4.30	alkyl, π−alkyl
		HIS106	5.10	alkyl, π−alkyl
ZINC000008764559	−9.8	ALA100	2.52	conventional HB
		ARG356	2.29, 2.52	conventional HB
		TYR32	3.42	carbon HB
		GLY28	2.86	carbon HB
		ASP173	3.99	π−anion
		VAL35	3.75, 3.96	π−σ
		PHE97	4.08	π−π stacked
		VAL27	5.34	alkyl, π−alkyl
		ALA50	4.29	alkyl, π−alkyl
		LYS52	5.13	alkyl, π−alkyl
		LEU158	5.13	alkyl, π−alkyl
		ILE79	4.79	alkyl, π−alkyl
		ALA172	4.28	alkyl, π−alkyl

https://doi.org/10.1021/acsomega.2c04837
ACS Omega 2023, 8, 391−409

Table 2. Lipinski's Rule of Five and Drug-Likeness Prediction of Top-Ranked Ligands

	Lipinski's rule of five										
compound ID	MW	mLog *P*	nHBA	nHBD	MR	Lipinski's violations	Lipinski's rule	TPSA	nRot	PAINS #alerts	Brenk #alerts
ZINC000005854718	406.47	2.64	5	3	121.43	0	yes	90.9	5	0	1
ZINC000013485410	390.47	3.2	4	2	119.41	0	yes	70.67	5	0	1
ZINC000005195832	338.35	1.64	5	3	97.71	0	yes	90.9	3	0	1
ZINC000002097716	453.48	2	7	2	124.41	0	yes	115.07	9	0	1
ZINC000013860547	370.35	0.56	7	5	101.75	0	yes	131.36	3	1	2
ZINC000020426551	411.4	0.55	7	3	110.05	0	yes	126.07	8	0	0
ZINC000012296886	369.32	−0.11	7	3	95.63	0	yes	126.07	7	0	0
ZINC000020763042	425.43	0.77	7	3	114.86	0	yes	126.07	9	0	0
ZINC000005831326	411.4	1.37	7	2	109.99	0	yes	115.07	8	0	1
ZINC000008764559	325.32	1.31	5	1	89.53	0	yes	79.98	4	0	0

varied temperatures are represented in Figure 6. RMSF is a numerical measurement of individual residue flexibility or how much a particular amino acid residue moves (fluctuates) during an MD simulation. The calculated RMSDs were re-evaluated using RMSF. The variations of amino acid residues observed in RMSF were aligned with the RMSD to compare the deviation and fluctuation in the complex structure. The residues indicating the highest fluctuation in the RMSF may be responsible for causing the deviation in the RMSD. The RMSF for 6T41−ZINC000005854718 was determined at 298, 300, 305, 310, and 320 K, as shown in Figure 7. The RMSF of 6T41−ZINC000005854718 per residue was plotted *versus* residue number. The RMSF plot of 6T41−ZINC000005854718 in 298 K represented that the GLU165 (RMSF value: 0.5314 nm) amino acid residue showed a slight fluctuation over 100 ns simulation. At 300 K, LEU252 (RMSF value: 0.6002 nm) and ASP253 (RMSF value: 0.6187 nm) amino acid residues showed fluctuations. The amino acid residue, LEU252 (RMSF value: 0.4973 nm), of 6T41−ZINC000005854718 fluctuated in simulation at 305 K. The RMSF of amino acid residues present in the targeted protein structure at body temperature (310 K) indicated fluctuation in GLU268 (RMSF value: 0.5717 nm), LYS271 (RMSF value: 0.584 nm), MET273 (RMSF value: 0.524 nm), and PHE346 (RMSF value: 0.8383 nm). As compared to the increased RMSD at body temperature (310 K), the minimum fluctuations in the RMSF plot confirmed the stable nature of the amino acid residues of CDK8 (PDB: 6T41). For the simulation at 320 K, THR229 (RMSF value: 0.5868 nm), SER230 (RMSF value: 0.4807 nm), and GLU231 (RMSF value: 0.5245 nm) amino acid residues showed fluctuations. However, the RMSF values of 6T41−ZINC000005854718 determined at varied temperature conditions remained in the acceptable range, indicating the stability of particular amino acid residues present in the protein structure. The RMSF and RMSD of 6T41−ZINC000005854718 at room temperature attained the maintained confirmation.

The conformational changes that occurred in the protein structure during the MD simulation were quantified with the help of the radius of gyration. The calculated R_g provided the average distance of all the scattered elements from the center of mass of the molecule. Moreover, the correlation between RMSD and RMSF with the obtained R_g provided insights into the impact of complex compressibility on the deviations in the complex RMSD and residual fluctuations observed in RMSF. The time evolution of R_g for the 6T41−ZINC000005854718 complex was studied over 100 ns at varied temperatures, and through the analysis, it is observed that the R_g values for 6T41−ZINC000005854718 in 300 K slightly get increased after 30 ns. The compactness of a complex system affects the residual fluctuations, and it further affects the complex stability. In the case of body temperature (310 K), R_g analysis showed consistent compressibility of 6T41−ZINC000005854718 after 20 ns with minimum fluctuation in the R_g value, as shown in Figure 8. Through the observed R_g, RMSD, and RMSF of 6T41−ZINC000005854718 in 310 K, it is clear that the complex compressibility did not cause significant residual fluctuation in RMSF, but some residues showed high RMSF values, and these residues may be responsible for the slightly increasing RMSD. The overall analysis of R_g for all the temperature-induced simulations of 6T41−ZINC000005854718 indicated the consistent compressibility of the complex system over 100 ns with negligible deviation in the plotted R_g values.

The number of HBs present between interactions of the protein and ligand plays an important role in the stability of that protein−ligand complex system. The HBs with R_g were correlated and analyzed over 100 ns at 298, 300, 305, 310, and 320 K simulation conditions. Figure 9 represents the time evaluation of intermolecular HBs over the 100 ns simulation. The simulation performed on the body temperature indicated the highest HB profile over the entire simulation period, and between 50 and 60 ns, the ligand showed the highest number of hydrogen formations with the residues of CDK8 (PDB: 6T41). The visualization of post-MD interaction at body temperature represented in Figure 10 confirmed the formation of a conventional HB interaction with ARG356 and PHE358, while HIS102 showed a carbon−HB interaction with the ligand group. The formed HBs may play a crucial role in stabilizing the compactness of the complex structure of the body temperature. Initially, interactions of the docked complex indicated a lack of conventional HBs after molecular docking (Figure 4), but the MD simulation study cleared the conventional HB interaction over 100 ns at 300, 350, 310, and 320 K.

Further, the simulated MD trajectories of 6T41−ZINC000005854718 at different temperatures were subjected to the confirmational PCA of C_α atoms. In the current work, PCA was done to determine the variability, collective motions, and changes in protein structural conformational states in the subsets of the principal components that appeared throughout the MD simulations. The results for the PCA study using MD trajectories of 6T41−ZINC000005854718 at 298, 300, 305, 310, and 320 K were carried out *via* the Bio3D package, and

https://doi.org/10.1021/acsomega.2c04837
ACS Omega 2023, 8, 391−409

Table 3. Predicted *In Silico* ADMET Properties for Top-Ranked Ligands

	absorption	distribution			metabolism							excretion	toxicity
					substrate		inhibitors						
	intestinal absorption (human)	VDss (human)	BBB permeability	CNS permeability			CYP					total clearance	AMES toxicity
compound ID	numeric (% absorbed)	numeric (log L kg^{-1})	numeric (log BB)	numeric (log PS)	2D6	3A4	1A2	2C19	2C9	2D6	3A4	numeric (log mL min^{-1} kg^{-1})	categorical (yes/no)
					categorical (yes/no)								
ZINC000005854718	92.312	−0.143	−1.037	−1.838	no	no	yes	yes	yes	no	no	0.543	no
ZINC000013485410	92.908	0.374	−0.092	−1.63	no	yes	yes	yes	yes	no	yes	0.459	no
ZINC000005195832	91.99	−0.043	−0.043	−2.054	no	no	yes	yes	yes	no	yes	0.512	no
ZINC000002097716	85.712	−0.249	−0.385	−0.385	no	yes	no	yes	yes	no	yes	0.207	no
ZINC000013860547	76.141	0.573	−1.511	−3.21	no	no	yes	no	no	no	no	0.308	no
ZINC000020426551	54.478	−1.244	−1.327	−3.67	no	no	no	no	no	no	no	0.706	no
ZINC000012296886	56.786	−0.632	−1.333	−3.848	no	yes	no	no	no	no	no	0.626	no
ZINC000020763042	55.171	−1.15	−1.353	−3.643	no	no	no	no	no	no	no	0.721	no
ZINC000005831326	85.389	−0.325	−0.546	−3.401	no	yes	no	yes	yes	no	yes	0.594	no
ZINC000008764559	94.615	−0.061	−0.204	−2.238	no	yes	yes	yes	no	no	yes	0.854	no

the obtained eigenvalues *versus* eigenvector plots are represented in Figure 11. The dominating motion from each trajectory is extracted in the smaller subset and further compared for the first three eigenvectors (PC1, PC2, and PC3). The color dots were used to represent the captured variance by eigenvectors and changing color from blue to white to red was used to indicate the time of sampling of the complex. Table 4 represents the dominating motion of 6T41−ZINC000005854718 at different temperatures extracted in the smaller subset and compared for the first three eigenvectors (PC1, PC2, and PC3). 6T41−ZINC000005854718 simulated at 310 K showed the highest variability in PC1 with regard to the internal motions of the MD trajectory. While 6T41−ZINC000005854718 simulated at 305 K showed the minimum variability in the PC2 statistics, and the resulting PC3 calculations for 6T41−ZINC000005854718 simulated at different temperatures showed minimum changes depicted from 6.17 to 8.2%.

2.5. Calculation of MM/PB(GB)SA and DelPhi Analysis. The highest negative values of binding affinity observed between the 6T41−ZINC000005854718 interaction (as shown in Table 1) indicated tight conformational binding. MM/PBSA using farPPI was utilized to analyze the binding free energy since only the docking score did not specify a satisfactory prediction for the binding affinity between the protein−ligand complex. The result for MM/PB(GB)SA using PB3, PB4, GB1, GB2, GB5, and GB6 methods indicated that the complex showed the highest negative binding free energy as compared to the binding affinity computed *via* molecular docking protocol. The binding free energy observed from MM/PB(GB)SA is more satisfactory, and the compared energies are represented in Table 5. Moreover, the corrected reaction field energy and Coulombic energy were calculated using the DelPhi webserver. The obtained corrected reaction field energy for 6T41−ZINC000005854718 at 298 K was found to be −1890.40 kT; at 300 K, it is −1882.32 kT; at 305 K, it is −1866.78 kT; at body temperature (310 K), it is −1897.23 kT; and at 320 K, it is −1823.29 kT. Similarly, the observed Coulombic energies are −38 275.43, −38 264.32, −38 258.01, −38 240.83, and −38 268.28 kT for 298, 300, 305, 310, and 320 K, respectively.

3. DISCUSSION

CDK8 plays a vital role in oncogenesis and has driven a major attraction as a therapeutic target.[35] Cyclin C bounded with CDK8 plays a crucial role in the regulation of transcription by the formation of a kinase module or transcription factor phosphorylation.[36] CDK8 and mediator complex serves as a molecular bridge between transcription factors, chromatin modifiers, promoters, enhancers, and RNA Polymerase II.[37] CDK8 plays a crucial role in cell proliferation and acts as an oncogene in colon cancer and its gene expression is associated with prognostication in the case of breast and ovarian cancers.[38] CDK8 participates in the transition process of epithelial-to-mesenchymal and that plays a vital role in the metastasis of breast cancer cells.[39] Breast cancer patients with shorter relapse-free survival have been reported to have increased level of CDK8 and its associated proteins, which was found to be activated in breast cancers and related to tumor progression.[40] In breast cancers, CDK8 facilitates and potentiates estrogen receptors which result in estrogen-induced phosphorylation of the carboxy-terminal domain of RNA Polymerase II at Ser2, which in turn assists the complete

https://doi.org/10.1021/acsomega.2c04837
ACS Omega 2023, 8, 391−409

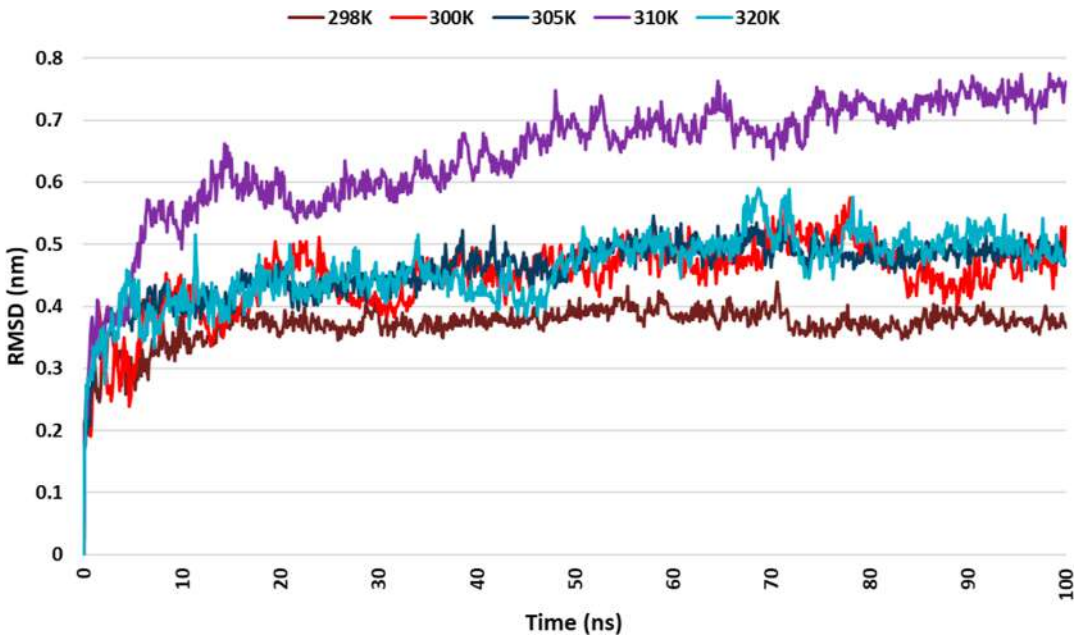

Figure 6. RMSDs of 6T41−ZINC000005854718 *vs* time (100 ns) at 298, 300, 305, 310, and 320 K.

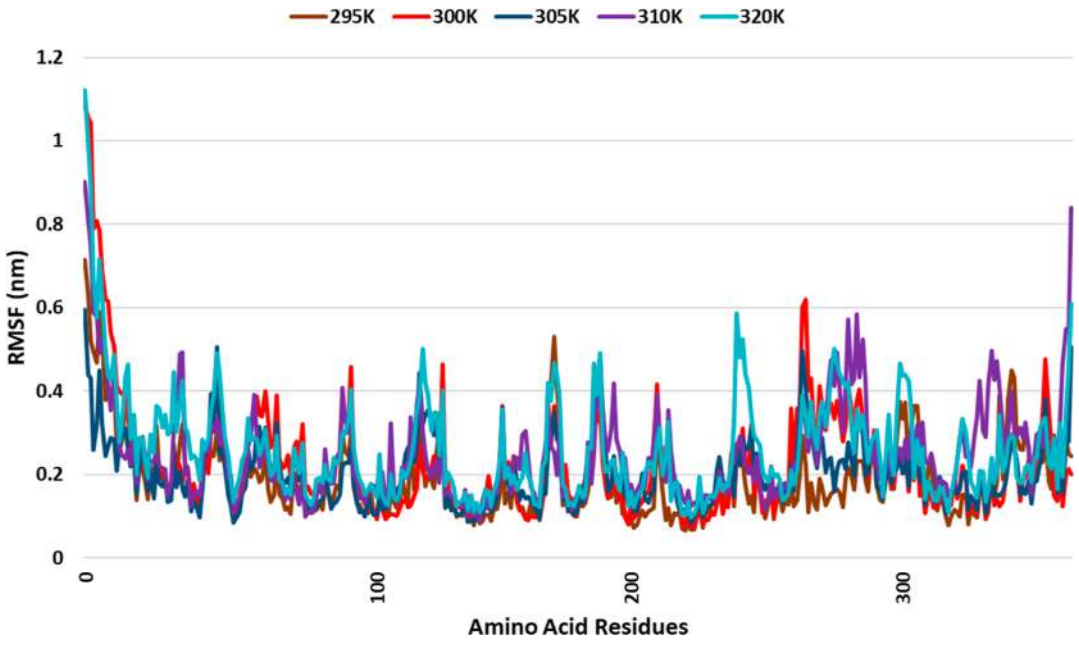

Figure 7. RMSFs of 6T41−ZINC000005854718 at 298, 300, 305, 310, and 320 K.

process of transcription of ER-inducible genes more effectively.[16] Due to the oncogenic potential of CDK8, the effective and selective inhibition of CDK8 is of great interest to develop a new therapeutic strategy.[41]

Computational screening techniques have tremendous applications in the drug discovery pipeline.[42] In the past few decades, molecular docking, *in silico* pharmacokinetic profiling, and MD simulations are extensively applied as computer-aided drug designing tools for identifying therapeutically important lead molecules.[43,44] The main aim of the study was to obtain a potential CDK8 inhibitor *via* the high-throughput computational exploration approach. Molecular docking is an important bioinformatics tool used for the prediction of binding confirmations along with the binding affinity of ligands against target proteins. The performed docking study provided important insights regarding the binding potential of subjected flavonoids and target protein. The binding affinities of docked flavonoids and used standards {CCT251545, ponatinib, linifanib, cortistatin A, and *N*-[(4-chlorophenyl)methyl]-quinazolin-4-amine} were compared, and through the comparison, it is observed that lupalbigenin (ZINC000005854718) and licoflavone B (ZINC000013485410) showed highest negative binding affinity than the compared standards. Previously, Ausawasamrit *et al.* reported an *in vitro* study on the anticancer activity of lupalbigenin against the protein kinase B (pAKT/AKT) and extracellular signal-regulated kinase (pERK/ERK).[45] Recently, in 2022, Shao *et al.* reported an investigation of the autophagic cell death-inducing ability of lupalbigenin on the SW480 cell line.[46] The CDK8 inhibitory mechanism of lupalbigenin and its

https://doi.org/10.1021/acsomega.2c04837
ACS Omega 2023, 8, 391−409

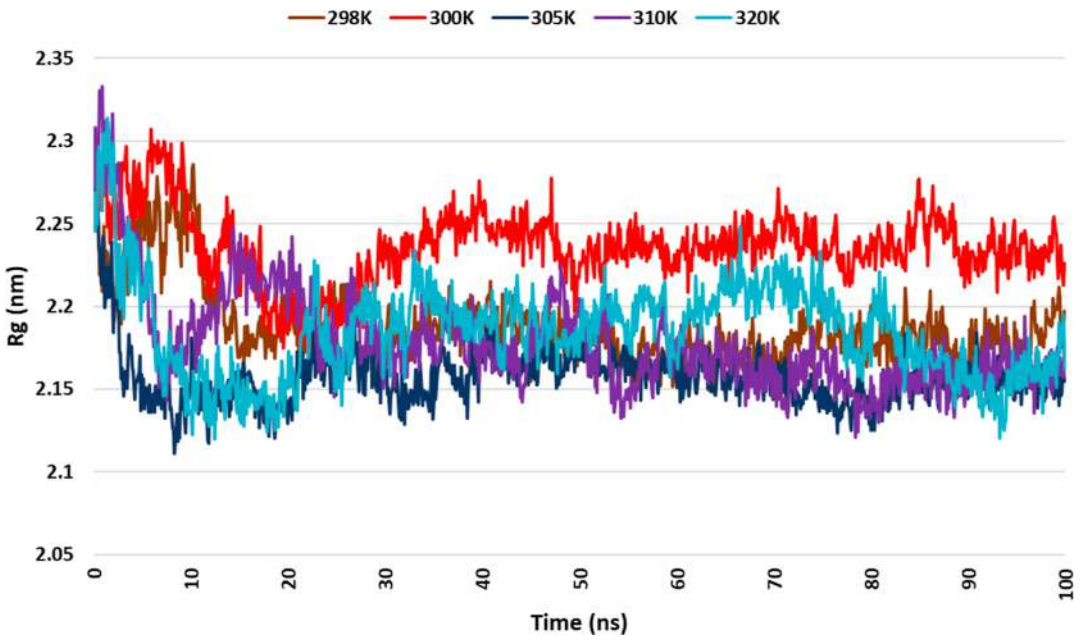

Figure 8. Radius of gyration (R_g) of 6T41−ZINC000005854718 *vs* time (100 ns) at 298, 300, 305, 310, and 320 K.

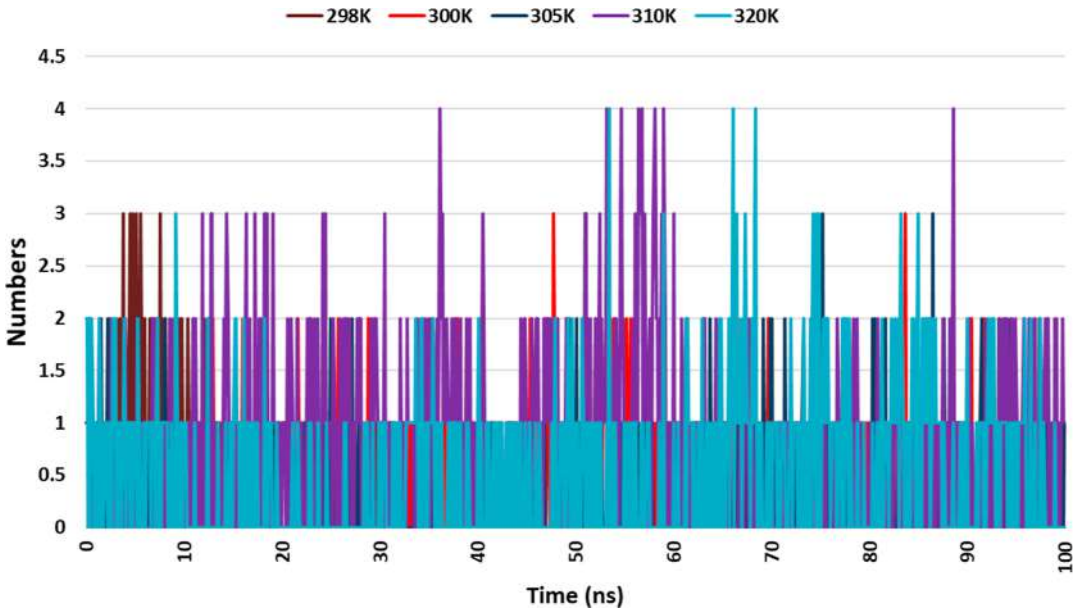

Figure 9. Intermolecular hydrogen bonding study plot for 100 ns MD simulation of 6T41−ZINC000005854718 at 298, 300, 305, 310, and 320 K.

stability with CDK8 are still unknown; hence, the behavior of lupalbigenin in a complex with CDK8 was explored in the current study. In all the docked ligands, the binding affinity of lupalbigenin was found at −10.7 kcal/mol, which is the highest negative binding affinity. Phytoconstituents isolated from the marine sponge *Corticium simplex* called cortistatin A is one of the reference drug used in this study to compare the docking results and Hatcher *et al.* reported the CDK8 inhibitory activity of cortistatin A.[47] The binding affinity for cortistatin A was found to be −10.1 kcal/mol, which is less as compared to the obtained hit, that is, lupalbigenin (ZINC000005854718). The pharmacokinetic profiling of 180 ligands with a binding affinity of more than −9 kcal/mol revealed that 91 ligands satisfied Lipinski's rule of five and ADMET requirements.

Further, the MD simulation study of the targeted empty protein structure and the protein−ligand complex with the highest negative binding affinity was carried out in varied temperature conditions to determine the effect of temperature on the structural rearrangement and the unfolding of the protein.[48−50] Previously, Rocco *et al.* performed a temperature-dependent MD simulation of protein structure to determine the unfolding processes of the simulated structure.[51] Similarly, Rath and Kumar studied the effect of temperature on the behavior of protein structure under an MD simulation study.[52] According to the study published by Dong *et al.*, the flexibility of protein may vary with the applied temperature conditions.[53] The MD simulation of the 6T41−ZINC000005854718 complex system in increasing temperature showed structural rearrangements, which may be caused by temperature

https://doi.org/10.1021/acsomega.2c04837
ACS Omega 2023, 8, 391−409

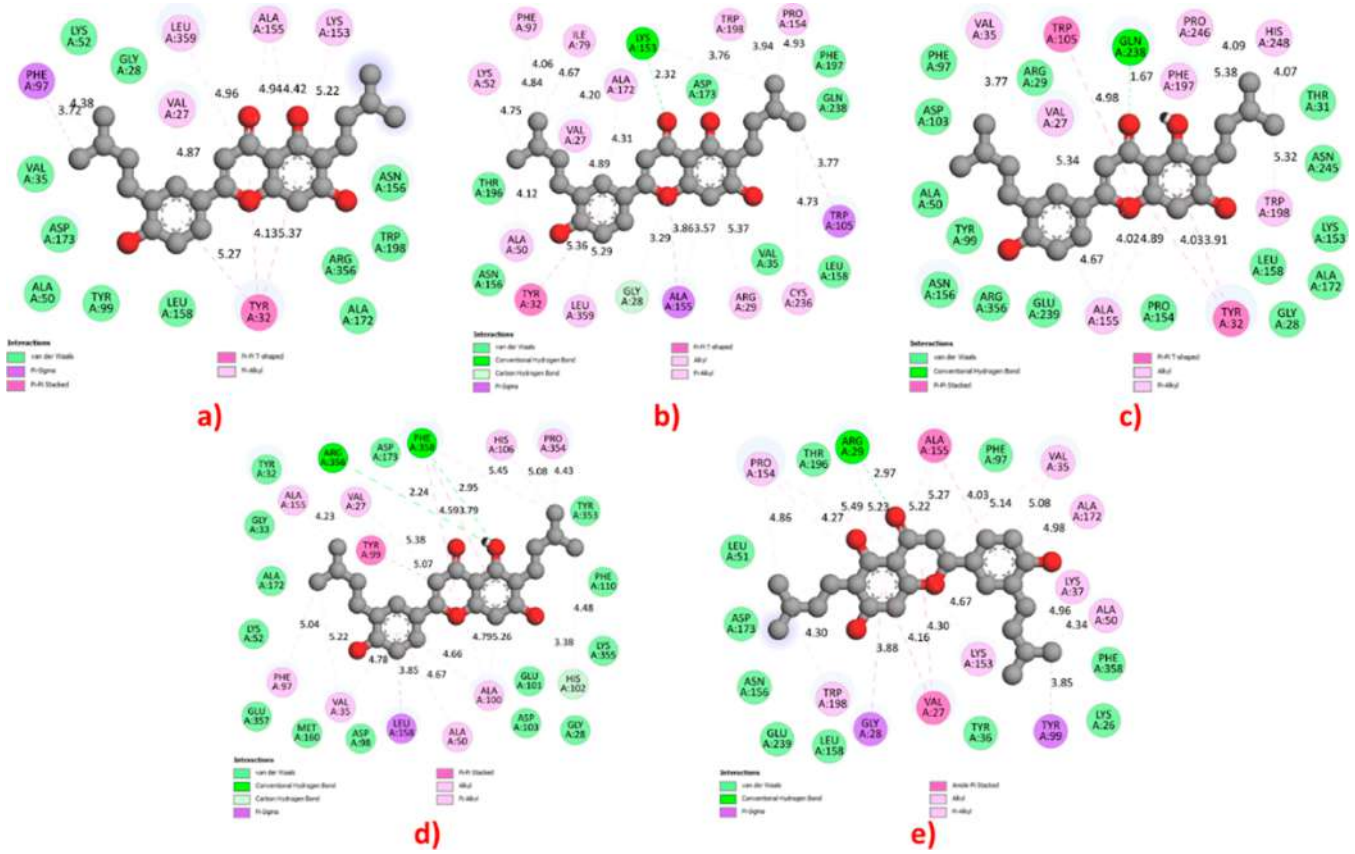

Figure 10. Post-MD simulation interactions of 6T41−ZINC000005854718 at (a) 298, (b) 300, (c) 305, (d) 310, and (e) 320 K.

variation. The simulation performed at body temperature (310 K) provided important insights regarding the stable nature of the complex system. PCA analysis and calculated Coulombic energy also contributed to clearing the stability of the complex systems. The overall computational study indicates the stability of lupalbigenin (ZINC000005854718) in complex with CDK8, but still more exploration of the hit molecule *via* the *in vitro* and *in vivo* study is needed to find out the anticancer activity of lupalbigenin against the CDK8 cells.

4. CONCLUSIONS

CDKs are one of the main regulators of the cell cycle and transcription, causing breast and related cancers. CDK has a huge family in which several CDKs are present, out of which CDK8 has been identified as a key oncogenic driver in various cancers. Flavonoids are a group of phytochemicals having a variety of phenolic structures with medicinal potential. In the current study, a total of 800 flavonoids were subjected to identify the potential ligand against CDK8. Modern CADD techniques such as molecular docking, virtual prediction of drug-likeness, ADMET prediction, and MD simulation were performed to identify the lead molecule. As per the molecular docking results, the binding affinity of selected flavonoids ranged between −5.5 and −10.7 kcal/mol. Out of all the docked ligands and standards, ZINC000005854718 showed the highest negative binding affinity of −10.7 kcal/mol with the targeted protein (PDB: 6T41). Similarly, it passed all the criteria to be a drug-like candidate without any toxicity; hence, it was subjected to MD simulation using five different conditions to determine the configurational changes occurring over the 100 ns. In the molecular dynamics simulation study, it was observed that the 6T41−ZINC000005854718 complex is stable in the simulation performed using body temperature (310 K). Moreover, the performed energetics study using MM/PB(GB)SA and DelPhi analysis suggested that the 6T41−ZINC000005854718 complex has a corrected reaction field energy of −1897.23 kT and a Coulombic energy of −38 275.43 kT, and energies observed *via* the MM/PB(GB)SA approach were found to be good compared to binding affinity. The binding free energy calculation indicated the tight binding between 6T41−ZINC000005854718. The results of the current study can be considered as an initial investigation; further *in vitro* or *in vivo* studies are necessary for the final confirmation and validation of the inhibitory activity of ZINC000005854718 against CDK8.

5. COMPUTATIONAL DETAILS

5.1. Protein and Ligand Preparation. The previously reported 3D crystal structure of CDK8 with PDB: 6T41 having 2.45 Å resolutions was retrieved from the RCSB Protein data bank (available at https://www.rcsb.org/).[40,41] Further, the downloaded protein structure was cleaned and prepared by removing water molecules and previously bound ligand groups. The binding pocket analysis and all the protein preparation tasks were done using BIOVIA Discovery Studio.[54] The prepared protein structure was subjected to validation and quality evaluation using the PROCHECK, ERRAT, PROVE, and Verify3D tools from the SAVES server (available at https://saves.mbi.ucla.edu/), and the online ProSA-web (available at https://prosa.services.came.sbg.ac.at/prosa.php) was used to determine the overall QMEAN score.[55−59] Further, the protein structure was protonated by the addition

https://doi.org/10.1021/acsomega.2c04837
ACS Omega 2023, 8, 391−409

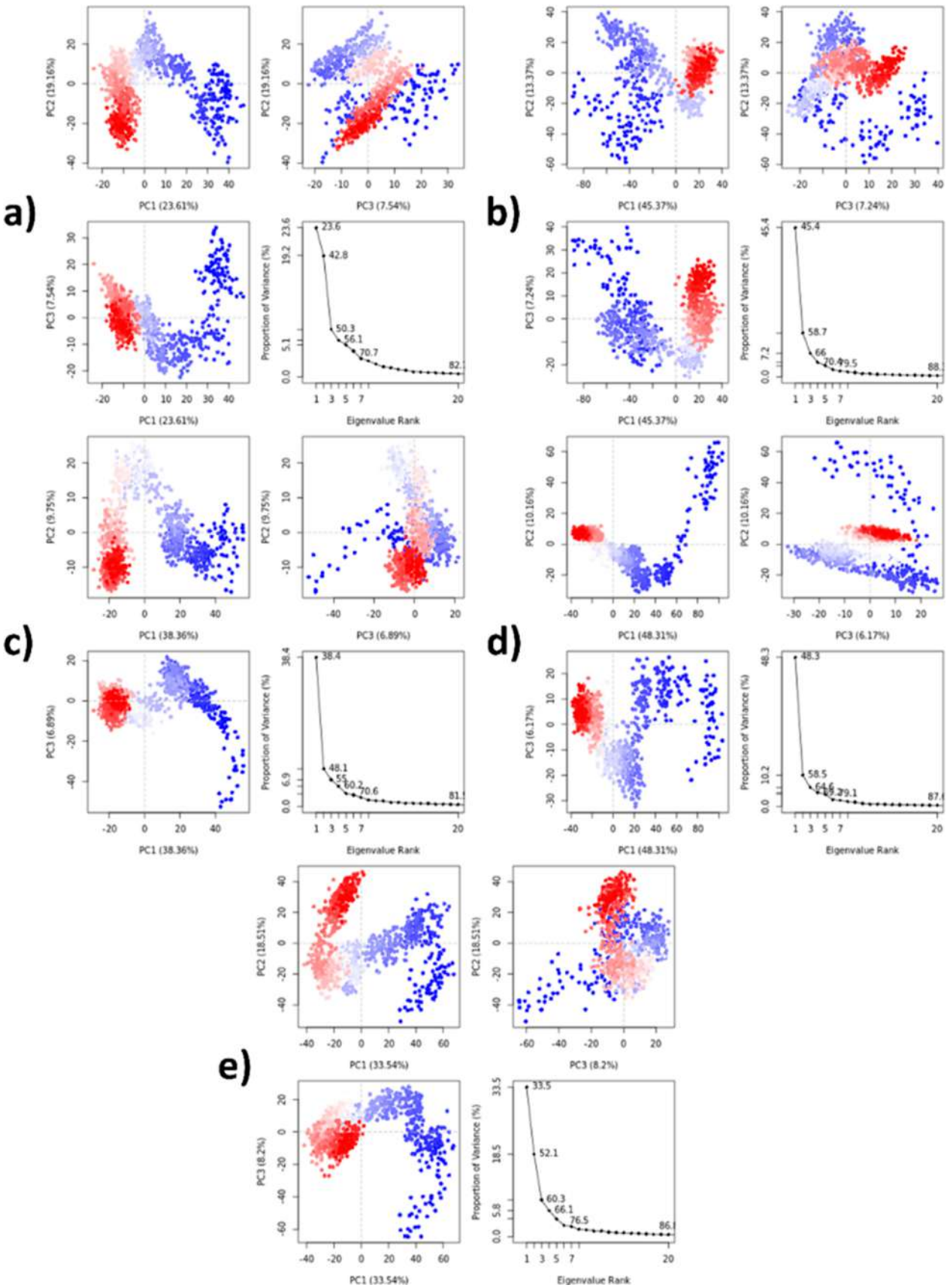

Figure 11. PCA of the MD trajectory of 6T41−ZINC000005854718 at (a) 298, (b) 300, (c) 305, (d) 310, and (e) 320 K. White dots indicate the intermediate state, blue dots with scattering represent the energetically unstable conformational state, and red dots indicate the stable conformational state.

https://doi.org/10.1021/acsomega.2c04837
ACS Omega 2023, 8, 391−409

Table 4. Variance in Principal Components Observed *via* PCA for 6T41−ZINC000005854718 at Different Temperatures

	principal components		
temperature (K)	PC1 (%)	PC2 (%)	PC3 (%)
298	23.6	19.13	7.54
300	45.4	13.37	7.24
305	38.4	9.75	6.89
310	48.3	10.16	6.17
320	33.5	18.51	8.2

Table 5. Calculated Energy Parameters for Each of the 6T41−ZINC000005854718 Complexes

energy type		energy (kcal/mol)
AutoDock Vina binding affinity		−10.7
MM/PB(GB)SA binding free energy	PB3	−18.42
	PB4	−25.2
	GB1	−40.23
	GB2	−41.05
	GB5	−45.08
	GB6	−30.91

of polar hydrogen atoms. Structures of over 800 flavonoids, including the flavones, isoflavones, flavanones, and flavonols, were downloaded from the Zinc Database (available at https://zinc.docking.org/substances/home/).[60,61] However, five previously reported CDK8 inhibitors (cortistatin A, CCT251545, ponatinib, and linifanib) and one co-crystalized ligand group from PDB: 6T41 {*N*-[(4-chlorophenyl)methyl]-quinazolin-4-amine} were used as standards to perform and compare the results of this *in silico* investigation.[35,62−64]

5.2. Molecular Docking Studies. Molecular docking was performed using the AutoDock Vina package of PyRx 0.8 (available at https://pyrx.sourceforge.io/).[34,65−67] The PDB file format of the target protein was loaded in PyRx 0.8 and then converted as a macromolecule in the PDBQT file format. The structure of ligands was subjected to energy minimization (EM) and converted to the PDBQT format using the OpenBabel plugin of PyRx.[68] The ligand structures and targeted protein were selected in AutoDock Vina, and a grid box was selected to cover the residues of the binding site, with dimensions *X*: 88.11 Å, *Y*: 66.97 Å, and *Z*: 88.78 Å and with center *X*: −4.8118, *Y*: −15.065, and *Z*: 28.1341 using the Vina workspace. The exhaustiveness was set to default at 8. Further, the best pose with minimum binding affinity and zero RMSD was selected for each ligand. Additionally, the interaction between docked protein and ligand was visualized, and saved conformations were analyzed with the help of BIOVIA Discovery Studio.

5.3. Drug-Likeness and *In Silico* ADMET. Drug-likeness of selected flavonoid structures was done by applying Lipinski's rule of five (Ro5). Lipinski's Ro5 is the most commonly used filter to sort the molecules based on their lead-likeness, and it helps to determine the oral absorptivity of compounds.[69] In the current work, the drug-likeness and ADMET properties of selected ligands were determined with the help of user-friendly online tools such as SwissADME (available at http://www.swissadme.ch/index.php)[70] and pkCSM (available at http://biosig.unimelb.edu.au/pkcsm/).[71] SwissADME gives the predictions of fundamental elements such as physicochemical properties, drug-likeness, and medicinal chemistry friendliness, while pkCSM provides the predictive models of central ADMET properties for drug development.

5.4. MD Simulation. MD simulation of the targeted empty protein structure, protein−standard complex, and best docked protein−ligand complex with the highest negative binding affinity was performed using the GROMACS simulation package *via* WebGRO (available at https://simlab.uams.edu/), and the GROMOS96 43a1 force field was selected.[72−75] Topology files of ligand were built using the GlycoBioChem PRODRG 2.5 (available at http://davapc1.bioch.dundee.ac.uk/cgi-bin/prodrg) server.[76,77] The simple point charge water model along with a triclinic box was chosen to solvate the protein−ligand complex system.[78] The EM of subjected complex systems was done using 5000 steps of the steepest descent algorithm and the protein−ligand complex was neutralized. The simulation was performed in the presence of 0.15 M NaCl.[79] Canonical (*NVT*) and isothermal−isobaric (*NPT*) ensembles after each step of EM were done to equilibrate the simulated systems.[80−82] The MD simulation of the protein−ligand complex was performed in different temperature conditions (298, 300, 305, 310, and 320 K), and each time, the temperature was maintained with the help of the Berendsen thermostat approach while the pressure was maintained at 1.0 bar using the Parrinello−Rahman barostat approach to control the entire simulated complex system in each temperature condition.[83−85] All the simulations were performed for 100 ns, and the obtained trajectories of MD simulation at different temperature conditions were used further for statistical analysis (RMSD, RMSF, R_g, and HBs).[86] The PCA analysis of the obtained MD trajectories was carried out using the Bio3D package *via* the Galaxy Australia server.[87−90]

5.5. Calculation of MM/PB(GB)SA and DelPhi Analysis. The protein−ligand binding free energy is calculated *via* the MM/PB(GB)SA methods using the farPPI webserver.[91] GAFF2 and ff14SB force fields for the ligand and protein were used in combination to perform the calculation. The binding free energy of the protein−ligand complex was calculated using the PB3, PB4, GB1, GB2, GB5, and GB6 procedure for MM/PB(GB)SA calculation.[92] The number followed by PB is a type of Poisson−Boltzmann calculation. The parameters applied for the procedure are the same as the workflow for automated MM-PBSA and MM-GBSA calculations in AmberTools17. The entire protocol was prepared and followed according to previously reported literature by Yalçın *et al.*,[93] Shephali *et al.*,[94] and Venkateshan *et al.*[95] The calculated binding free energy of the protein−ligand complex is based on the equation previously reported by Mohapatra *et al.*[96] Moreover, the Coulombic energies were calculated for the simulated complex at all the temperatures using the DelPhi C++ V. 8.4 implemented *via* the Delphi Webserver (available at http://compbio.clemson.edu/sapp/delphi_webserver/) which is an online Poisson−Boltzmann solver to calculate the electrostatic energies and potential of biological macromolecules.[97]

■ ASSOCIATED CONTENT

Supporting Information

The Supporting Information is available free of charge at https://pubs.acs.org/doi/10.1021/acsomega.2c04837.

Docking, drug-likeness, *in silico* ADMET, and MD simulation studies (PDF)

https://doi.org/10.1021/acsomega.2c04837
ACS Omega 2023, 8, 391−409

AUTHOR INFORMATION

Corresponding Author

Sanket Rathod − *Department of Pharmaceutical Chemistry, Bharati Vidyapeeth College of Pharmacy, Kolhapur 416 013 Maharashtra, India;* orcid.org/0000-0002-8037-5974; Phone: +91 8855045618; Email: sanket.rathod-copk@bvp.edu.in, ssrathod7588@gmail.com

Authors

Ketaki Shinde − *Department of Quality Assurance Techniques, Poona College of Pharmacy, Bharati Vidyapeeth Deemed University, Pune 411 038 Maharashtra, India*

Jaykedar Porlekar − *Department of Pharmaceutics, Bharati Vidyapeeth College of Pharmacy, Kolhapur 416 013 Maharashtra, India*

Prafulla Choudhari − *Department of Pharmaceutical Chemistry, Bharati Vidyapeeth College of Pharmacy, Kolhapur 416 013 Maharashtra, India*

Rakesh Dhavale − *Department of Pharmaceutics, Bharati Vidyapeeth College of Pharmacy, Kolhapur 416 013 Maharashtra, India*

Deepak Mahuli − *Department of Pharmacology, Bharati Vidyapeeth College of Pharmacy, Kolhapur 416 013 Maharashtra, India*

Yasinalli Tamboli − *Wockhardt Research Centre, Aurangabad 431 006 Maharashtra, India;* orcid.org/0000-0002-5161-0170

Manish Bhatia − *Department of Pharmaceutical Chemistry, Bharati Vidyapeeth College of Pharmacy, Kolhapur 416 013 Maharashtra, India*

Kishan P. Haval − *Department of Chemistry, Dr. Babasaheb Ambedkar Marathwada University Sub Campus, Osmanabad 413501 Maharashtra, India;* orcid.org/0000-0002-2526-8738

Abdullah G. Al-Sehemi − *Department of Chemistry, King Khalid University, Abha 61413, Saudi Arabia;* orcid.org/0000-0002-6793-3038

Mehboobali Pannipara − *Department of Chemistry, King Khalid University, Abha 61413, Saudi Arabia*

Complete contact information is available at: https://pubs.acs.org/10.1021/acsomega.2c04837

Author Contributions

CRediT authorship contribution: **Sanket Rathod** contributed to investigation, conceptualization, methodology, software, writing—original draft, writing—review and editing, and visualization. **Ketaki Shinde** contributed to investigation, data curation, and writing—original draft. **Jaykedar Porlekar** contributed to formal analysis and data curation. **Prafulla Choudhari** contributed to conceptualization, methodology, validation, formal analysis, data curation, writing—review and editing, and supervision. **Rakesh Dhavale** contributed to validation, formal analysis, writing—review and editing, and supervision. **Deepak Mahuli** contributed to writing—review and editing, and supervision. **Yasinalli Tamboli** contributed to resources, writing—review and editing, and supervision. **Manish Bhatia** contributed to writing—review and editing and supervision. **Kishan P Haval** contributed to writing—review and editing and supervision. **Abdullah G Al-Sehemi** contributed to writing—review and editing and supervision. **Mehboobali Pannipara** contributed to writing—review and editing and supervision.

Notes

The authors declare no competing financial interest.

ACKNOWLEDGMENTS

The authors are thankful to the Deanship of scientific research at King Khalid University and greatly appreciated for funding of this work under grant number R.G.P-2/179/43.

REFERENCES

(1) Drescher, C. W.; Bograd, A. J.; Chang, S. C.; Weerasinghe, R. K.; Vita, A.; Bell, R. B. Cancer Case Trends Following the Onset of the COVID-19 Pandemic: A Community-Based Observational Study with Extended Follow-Up. *Cancer* **2022**, *128*, 1475−1482.

(2) Hassanpour, S. H.; Dehghani, M. Review of Cancer from Perspective of Molecular. *J. Cancer Res. Pract.* **2017**, *4*, 127−129.

(3) Davis, E. J.; Beebe-Dimmer, J. L.; Yee, C. L.; Cooney, K. A. Risk of Second Primary Tumors in Men Diagnosed with Prostate Cancer: A Population-Based Cohort Study. *Cancer* **2014**, *120*, 2735−2741.

(4) Rahib, L.; Smith, B. D.; Aizenberg, R.; Rosenzweig, A. B.; Fleshman, J. M.; Matrisian, L. M. Projecting Cancer Incidence and Deaths to 2030: The Unexpected Burden of Thyroid, Liver, and Pancreas Cancers in the United States. *Cancer Res.* **2014**, *74*, 2913−2921.

(5) Brito, M. B.; Nobre, F.; Sales Vieira, C. Clinical Update Hormonal Contraception and Cardiovascular System. *Clin. Update* **2011**, *96*, e81−e89.

(6) Siegel, R. L.; Miller, K. D.; Fuchs, H. E.; Jemal, A. Cancer Statistics, 2022. *Ca-Cancer J. Clin.* **2022**, *72*, 7−33.

(7) Howell, A.; Anderson, A. S.; Clarke, R. B.; Duffy, S. W.; Evans, G.; Garcia-Closas, M.; Gescher, A. J.; Key, T. J.; Saxton, J. M.; Harvie, M. N. Risk Determination and Prevention of Breast Cancer. *Breast Cancer Res.* **2014**, *16*, 446.

(8) Feng, Y.; Spezia, M.; Huang, S.; Yuan, C.; Zeng, Z.; Zhang, L.; Ji, X.; Liu, W.; Huang, B.; Luo, W.; Liu, B.; Lei, Y.; Du, S.; Vuppalapati, A.; Luu, H. H.; Haydon, R. C.; He, T. C.; Ren, G. Breast Cancer Development and Progression: Risk Factors, Cancer Stem Cells, Signaling Pathways, Genomics, and Molecular Pathogenesis. *Genes Dis.* **2018**, *5*, 77−106.

(9) Kelsey, J. L.; Berkowitz, G. S. Breast Cancer Epidemiology. *Cancer Res.* **1988**, *48*, 5615−5623.

(10) Waks, A. G.; Winer, E. P. Breast Cancer Treatment: A Review. *JAMA, J. Am. Med. Assoc.* **2019**, *321*, 288−300.

(11) Sánchez-Martínez, C.; Lallena, M. J.; Sanfeliciano, S. G.; de Dios, A. Cyclin Dependent Kinase (CDK) Inhibitors as Anticancer Drugs: Recent Advances (2015−2019). *Bioorg. Med. Chem. Lett.* **2019**, *29*, 126637.

(12) Nandi, S.; Dey, R.; Dey, S.; Samadder, A.; Saxena, A. K. Naturally Sourced CDK Inhibitors and Current Trends in Structure-Based Synthetic Anticancer Drug Design by Crystallography. *Anticancer Agents Med. Chem.* **2022**, *22*, 485−498.

(13) Tutone, M.; Almerico, A. M. Recent Advances on CDK Inhibitors: An Insight by Means of in Silico Methods. *Eur. J. Med. Chem.* **2017**, *142*, 300−315.

(14) Zhang, M.; Zhang, L.; Hei, R.; Li, X.; Cai, H.; Wu, X.; Zheng, Q.; Cai, C. CDK Inhibitors in Cancer Therapy, an Overview of Recent Development. *Am. J. Cancer Res.* **2021**, *11*, 1913−1935.

(15) Malumbres, M. Cyclin-Dependent Kinases. *Genome Biol.* **2014**, *15*, 122.

(16) Philip, S.; Kumarasiri, M.; Teo, T.; Yu, M.; Wang, S. Cyclin-Dependent Kinase 8: A New Hope in Targeted Cancer Therapy? *J. Med. Chem.* **2018**, *61*, 5073−5092.

(17) Solum, E.; Hansen, T. V.; Aesoy, R.; Herfindal, L. New CDK8 Inhibitors as Potential Anti-Leukemic Agents—Design, Synthesis and Biological Evaluation. *Bioorg. Med. Chem.* **2020**, *28*, 115461.

(18) Silva-García, O.; Valdez-Alarcón, J. J.; Baizabal-Aguirre, V. M. Wnt/β-Catenin Signaling as a Molecular Target by Pathogenic Bacteria. *Front. Immunol.* **2019**, *10*, 2135.

(19) Lu, M. F.; Xiao, Z. T.; Zhang, H. Y. Where Do Health Benefits of Flavonoids Come from? Insights from Flavonoid Targets and Their Evolutionary History. *Biochem. Biophys. Res. Commun.* **2013**, *434*, 701−704.
(20) Cook, N. Flavonoids-Chemistry, Metabolism, Cardioprotective Effects, and Dietary Sources. *J. Nutr. Biochem.* **1996**, *7*, 66−76.
(21) Ahmad, A.; Kaleem, M.; Ahmed, Z.; Shafiq, H. Therapeutic Potential of Flavonoids and Their Mechanism of Action against Microbial and Viral Infections-A Review. *Food Res. Int.* **2015**, *77*, 221−235.
(22) Wang, T.-Y.; Li, Q.; Bi, K.-S. Bioactive Flavonoids in Medicinal Plants: Structure, Activity and Biological Fate. *Asian J. Pharm. Sci.* **2018**, *13*, 12−23.
(23) Khan, J.; Deb, P.; Priya, S.; Medina, K. D.; Devi, R.; Walode, S. G.; Rudrapal, M. Dietary Flavonoids: Cardioprotective Potential with Antioxidant and Their Pharmacokinetic, Toxicological and Therapeutic Concerns. *Molecules* **2021**, *26*, 4021.
(24) Maleki, S. J.; Crespo, J. F.; Cabanillas, B. Anti-Inflammatory Effects of Flavonoids. *Food Chem.* **2019**, *299*, 125124.
(25) Sarian, M. N.; Ahmed, Q.; Mat So'ad, S.; Alhassan, A.; Murugesu, S.; Perumal, V.; Syed Mohamad, S.; Khatib, A.; Latip, J. Antioxidant and Antidiabetic Effects of Flavonoids: A Structure-Activity Relationship Based Study. *BioMed Res. Int.* **2017**, *2017*, 8386065.
(26) Panche, A. N.; Diwan, A. D.; Chandra, S. R. Flavonoids: An Overview. *J. Nutr. Sci.* **2016**, *5*, No. e47.
(27) Kumar, S.; Pandey, A. K. Chemistry and Biological Activities of Flavonoids: An Overview. *Sci. World J.* **2013**, *2013*, 162750.
(28) Brogi, S.; Ramalho, T. C.; Kuca, K.; Medina-Franco, J. L.; Valko, M. Editorial: In Silico Methods for Drug Design and Discovery. *Front. Chem.* **2020**, *8*, 612.
(29) Ou-Yang, S. S.; Lu, J. Y.; Kong, X. Q.; Liang, Z. J.; Luo, C.; Jiang, H. Computational Drug Discovery. *Acta Pharmacol. Sin.* **2012**, *33*, 1131−1140.
(30) Katsila, T.; Spyroulias, G. A.; Patrinos, G. P.; Matsoukas, M. T. Computational Approaches in Target Identification and Drug Discovery. *Comput. Struct. Biotechnol. J.* **2016**, *14*, 177−184.
(31) Roy, H.; Nandi, S. In-Silico Modeling in Drug Metabolism and Interaction: Current Strategies of Lead Discovery. *Curr. Pharm. Des.* **2019**, *25*, 3292−3305.
(32) Nandi, S.; Bagchi, M. C. 3D-QSAR and Molecular Docking Studies of 4-Anilinoquinazoline Derivatives: A Rational Approach to Anticancer Drug Design. *Mol. Diversity* **2009**, *14*, 27−38.
(33) Jain, A. S.; Sushma, P.; Dharmashekar, C.; Beelagi, M. S.; Prasad, S. K.; Shivamallu, C.; Prasad, A.; Syed, A.; Marraiki, N.; Prasad, K. S. In Silico Evaluation of Flavonoids as Effective Antiviral Agents on the Spike Glycoprotein of SARS-CoV-2. *Saudi J. Biol. Sci.* **2021**, *28*, 1040−1051.
(34) Eberhardt, J.; Santos-Martins, D.; Tillack, A. F.; Forli, S. AutoDock Vina 1.2.0: New Docking Methods, Expanded Force Field, and Python Bindings. *J. Chem. Inf. Model.* **2021**, *61*, 3891−3898.
(35) Dale, T.; Clarke, P. A.; Esdar, C.; Waalboer, D.; Adeniji-Popoola, O.; Ortiz-Ruiz, M. J.; Mallinger, A.; Samant, R. S.; Czodrowski, P.; Musil, D.; Schwarz, D.; Schneider, K.; Stubbs, M.; Ewan, K.; Fraser, E.; TePoele, R.; Court, W.; Box, G.; Valenti, M.; de Haven Brandon, A.; Gowan, S.; Rohdich, F.; Raynaud, F.; Schneider, R.; Poeschke, O.; Blaukat, A.; Workman, P.; Schiemann, K.; Eccles, S. A.; Wienke, D.; Blagg, J. A Selective Chemical Probe for Exploring the Role of CDK8 and CDK19 in Human Disease. *Nat. Chem. Biol.* **2015**, *11*, 973−980.
(36) Wu, D.; Zhang, Z.; Chen, X.; Yan, Y.; Liu, X. Angel or Devil ?—CDK8 as the New Drug Target. *Eur. J. Med. Chem.* **2021**, *213*, 113043.
(37) Chen, B.; Wen, P.; Hu, G.; Gao, Y.; Qi, X.; Zhu, K.; Chen, S.; Wu, L.; Xu, A.; Zhao, G. Antagonizing CDK8 Sensitizes Colorectal Cancer to Radiation Through Potentiating the Transcription of E2f1 Target Gene Apaf1. *Front. Cell Dev. Biol.* **2020**, *8*, 408.
(38) Cholko, T.; Chen, W.; Tang, Z.; Chang, C.-E. A. A Molecular Dynamics Investigation of CDK8/CycC and Ligand Binding: Conformational Flexibility and Implication in Drug Discovery. *J. Comput.-Aided Mol. Des.* **2018**, *32*, 671−685.
(39) Knab, V. M.; Gotthardt, D.; Klein, K.; Grausenburger, R.; Heller, G.; Menzl, I.; Prinz, D.; Trifinopoulos, J.; List, J.; Fux, D.; Witalisz-Siepracka, A.; Sexl, V. Triple-Negative Breast Cancer Cells Rely on Kinase-Independent Functions of CDK8 to Evade NK-Cell-Mediated Tumor Surveillance. *Cell Death Dis.* **2021**, *12*, 991.
(40) Jha, V.; Devkar, S.; Gharat, K.; Kasbe, S.; Matharoo, D. K.; Pendse, S.; Bhosale, A.; Bhargava, A. Screening of Phytochemicals as Potential Inhibitors of Breast Cancer Using Structure Based Multitargeted Molecular Docking Analysis. *Phytomedicine Plus* **2022**, *2*, 100227.
(41) Klatt, F.; Leitner, A.; Kim, I. v.; Ho-Xuan, H.; Schneider, E. v.; Langhammer, F.; Weinmann, R.; Müller, M. R.; Huber, R.; Meister, G.; Kuhn, C. D. A Precisely Positioned MED12 Activation Helix Stimulates CDK8 Kinase Activity. *Proc. Natl. Acad. Sci. U.S.A.* **2020**, *117*, 2894−2905.
(42) Choudhury, C.; Arul Murugan, N.; Priyakumar, U. D. Structure-Based Drug Repurposing: Traditional and Advanced AI/ML-Aided Methods. *Drug Discovery Today* **2022**, *27*, 1847−1861.
(43) Salmaso, V.; Moro, S. Bridging Molecular Docking to Molecular Dynamics in Exploring Ligand-Protein Recognition Process: An Overview. *Front. Pharmacol.* **2018**, *9*, 923.
(44) Wan, H. What ADME Tests Should Be Conducted for Preclinical Studies? *ADMET DMPK* **2013**, *1*, 19−28.
(45) Ausawasamrit, A.; Itthiwarapornkul, N.; Chaotham, C.; Sukrong, S.; Chanvorachote, P. Lupalbigenin from Derris Scandens Sensitizes Detachment-Induced Cell Death in Human Lung Cancer Cells. *Anticancer Res.* **2015**, *35*, 2827−2834.
(46) Shao, X.; Chen, X.; Wang, Z.; Zhu, C.; Du, Y.; Tang, D.; Ji, S. Diprenylated Flavonoids from Licorice Induce Death of SW480 Colorectal Cancer Cells by Promoting Autophagy: Activities of Lupalbigenin and 6,8-Diprenylgenistein. *J. Ethnopharmacol.* **2022**, *296*, 115488.
(47) Hatcher, J. M.; Wang, E. S.; Johannessen, L.; Kwiatkowski, N.; Sim, T.; Gray, N. S. Development of Highly Potent and Selective Steroidal Inhibitors and Degraders of CDK8. *ACS Med. Chem. Lett.* **2018**, *9*, 540−545.
(48) Julió Plana, L.; Nadra, A. D.; Estrin, D. A.; Luque, F. J.; Capece, L. Thermal Stability of Globins: Implications of Flexibility and Heme Coordination Studied by Molecular Dynamics Simulations. *J. Chem. Inf. Model.* **2019**, *59*, 441−452.
(49) Lowen, A. C.; Steel, J. Roles of Humidity and Temperature in Shaping Influenza Seasonality. *J. Virol.* **2014**, *88*, 7692−7695.
(50) Kumar, S.; Deshpande, P. A. Structural and Thermodynamic Analysis of Factors Governing the Stability and Thermal Folding/Unfolding of SazCA. *PLoS One* **2021**, *16*, No. e0249866.
(51) Rocco, A. G.; Mollica, L.; Ricchiuto, P.; Baptista, A. M.; Gianazza, E.; Eberini, I. Characterization of the Protein Unfolding Processes Induced by Urea and Temperature. *Biophys. J.* **2008**, *94*, 2241−2251.
(52) Rath, S. L.; Kumar, K. Investigation of the Effect of Temperature on the Structure of SARS-CoV-2 Spike Protein by Molecular Dynamics Simulations. *Front. Mol. Biosci.* **2020**, *7*, 583523.
(53) Dong, Y. W.; Liao, M. L.; Meng, X. L.; Somero, G. N. Structural Flexibility and Protein Adaptation to Temperature: Molecular Dynamics Analysis of Malate Dehydrogenases of Marine Molluscs. *Proc. Natl. Acad. Sci. U.S.A.* **2018**, *115*, 1274−1279.
(54) Dassault Systèmes. *BIOVIA Discovery Studio Visualizr*; Dassault Systèmes: San Diego, 2020.
(55) Hashemzadeh, P.; Ghorbanzadeh, V.; Lashgarian, H. E.; Kheirandish, F.; Dariushnejad, H. Harnessing Bioinformatic Approaches to Design Novel Multi-Epitope Subunit Vaccine Against Leishmania Infantum. *Int. J. Pept. Res. Ther.* **2020**, *26*, 1417−1428.
(56) Dym, O.; Eisenberg, D.; Yeates, T. O. Detection of Errors in Protein Models. *International Tables for Crystallography Volume F: Crystallography of Biological Macromolecules*; Springer, 2006; pp 520−530.

https://doi.org/10.1021/acsomega.2c04837
ACS Omega 2023, 8, 391−409

(57) Bhowmik, D.; Nandi, R.; Prakash, A.; Kumar, D. Evaluation of Flavonoids as 2019-NCoV Cell Entry Inhibitor through Molecular Docking and Pharmacological Analysis. *Heliyon* **2021**, *7*, No. e06515.
(58) Wiederstein, M.; Sippl, M. J. ProSA-Web: Interactive Web Service for the Recognition of Errors in Three-Dimensional Structures of Proteins. *Nucleic Acids Res.* **2007**, *35*, W407−W410.
(59) Laskowski, R. A.; Macarthur, M. W.; Thornton, J. M. PROCHECK: A Program to Check the Stereochemical Quality of Protein Structures. *J. Appl. Cryst.* **1993**, *26*, 283−291.
(60) Irwin, J. J.; Sterling, T.; Mysinger, M. M.; Bolstad, E. S.; Coleman, R. G. ZINC: A Free Tool to Discover Chemistry for Biology. *J. Chem. Inf. Model.* **2012**, *52*, 1757−1768.
(61) Irwin, J. J.; Shoichet, B. K. ZINC-A Free Database of Commercially Available Compounds for Virtual Screening. *J. Chem. Inf. Model.* **2005**, *45*, 177−182.
(62) Cee, V. J.; Chen, D. Y.-K.; Lee, M. R.; Nicolaou, K. C. Cortistatin A Is a High-Affinity Ligand of Protein Kinases ROCK, CDK8, and CDK11. *Angew. Chem.* **2009**, *121*, 9114−9119.
(63) Hatcher, J. M.; Wang, E. S.; Johannessen, L.; Kwiatkowski, N.; Sim, T.; Gray, N. S. Development of Highly Potent and Selective Steroidal Inhibitors and Degraders of CDK8. *ACS Med. Chem. Lett.* **2018**, *9*, 540−545.
(64) Mallinger, A.; Schiemann, K.; Rink, C.; Stieber, F.; Calderini, M.; Crumpler, S.; Stubbs, M.; Adeniji-Popoola, O.; Poeschke, O.; Busch, M.; Czodrowski, P.; Musil, D.; Schwarz, D.; Ortiz-Ruiz, M. J.; Schneider, R.; Thai, C.; Valenti, M.; de Haven Brandon, A.; Burke, R.; Workman, P.; Dale, T.; Wienke, D.; Clarke, P. A.; Esdar, C.; Raynaud, F. I.; Eccles, S. A.; Rohdich, F.; Blagg, J. Discovery of Potent, Selective, and Orally Bioavailable Small-Molecule Modulators of the Mediator Complex-Associated Kinases CDK8 and CDK19. *J. Med. Chem.* **2016**, *59*, 1078−1101.
(65) Stanzione, F.; Giangreco, I.; Cole, J. C. Use of Molecular Docking Computational Tools in Drug Discovery. *Prog. Med. Chem.* **2021**, *60*, 273−343.
(66) Ikwu, F. A.; Isyaku, Y.; Obadawo, B. S.; Lawal, H. A.; Ajibowu, S. A. In Silico Design and Molecular Docking Study of CDK2 Inhibitors with Potent Cytotoxic Activity against HCT116 Colorectal Cancer Cell Line. *J. Genet. Eng. Biotechnol.* **2020**, *18*, 51.
(67) Dallakyan, S.; Olson, A. J. Small-Molecule Library Screening by Docking with PyRx. *Methods Mol. Biol.* **2015**, *1263*, 243−250.
(68) O'Boyle, N. M.; Banck, M.; James, C. A.; Morley, C.; Vandermeersch, T.; Hutchison, G. R. Open Babel: An Open Chemical Toolbox. *J. Cheminform.* **2011**, *3*, 33.
(69) Lipinski, C. A.; Dominy, B. W.; Feeney, P. J. Experimental and Computational Approaches to Estimate Solubility and Permeability in Drug Discovery and Development Settings. *Adv. Drug Delivery Rev.* **1997**, *23*, 3−25.
(70) Daina, A.; Michielin, O.; Zoete, V. SwissADME: A Free Web Tool to Evaluate Pharmacokinetics, Drug-Likeness and Medicinal Chemistry Friendliness of Small Molecules OPEN. *Sci. Rep.* **2017**, *7*, 42717.
(71) Pires, D. E. v.; Blundell, T. L.; Ascher, D. B. PkCSM: Predicting Small-Molecule Pharmacokinetic and Toxicity Properties Using Graph-Based Signatures. *J. Med. Chem.* **2015**, *58*, 4066−4072.
(72) Pol-Fachin, L.; Fernandes, C. L.; Verli, H. GROMOS96 43a1 Performance on the Characterization of Glycoprotein Conformational Ensembles through Molecular Dynamics Simulations. *Carbohydr. Res.* **2009**, *344*, 491−500.
(73) WebGrolUAMS. https://simlab.uams.edu/ (accessed May 23, 2022).
(74) Kalimuthu, A. K.; Panneerselvam, T.; Pavadai, P.; Pandian, S. R. K.; Sundar, K.; Murugesan, S.; Ammunje, D. N.; Kumar, S.; Arunachalam, S.; Kunjiappan, S. Pharmacoinformatics-Based Investigation of Bioactive Compounds of Rasam (South Indian Recipe) against Human Cancer. *Sci. Rep.* **2021**, *11*, 21488.
(75) Tumskiy, R. S.; Tumskaia, A. v. Multistep Rational Molecular Design and Combined Docking for Discovery of Novel Classes of Inhibitors of SARS-CoV-2 Main Protease 3CLpro. *Chem. Phys. Lett.* **2021**, *780*, 138894.
(76) Schüttelkopf, A. W.; van Aalten, D. M. F. PRODRG: A Tool for High-Throughput Crystallography of Protein-Ligand Complexes. *Acta Crystallogr., Sect. D: Biol. Crystallogr.* **2004**, *60*, 1355−1363.
(77) Raman, A. P. S.; Kumari, K.; Jain, P.; Vishvakarma, V. K.; Kumar, A.; Kaushik, N.; Choi, E. H.; Kaushik, N. K.; Singh, P. In Silico Evaluation of Binding of 2-Deoxy-D-Glucose with Mpro of NCoV to Combat COVID-19. *Pharmaceutics* **2022**, *14*, 135.
(78) Izadi, S.; Anandakrishnan, R.; Onufriev, A. v. Building Water Models: A Different Approach. *J. Phys. Chem. Lett.* **2014**, *5*, 3863.
(79) Gorai, S.; Junghare, V.; Kundu, K.; Gharui, S.; Kumar, M.; Patro, B. S.; Nayak, S. K.; Hazra, S.; Mula, S. Synthesis of Dihydrobenzofuro[3,2-b]Chromenes as Potential 3CLpro Inhibitors of SARS-CoV-2: A Molecular Docking and Molecular Dynamics Study. *ChemMedChem* **2022**, *17*, No. e202100782.
(80) Nosé, S. A Molecular Dynamics Method for Simulations in the Canonical Ensemble. *Mol. Phys.* **2002**, *100*, 191−198.
(81) Huang, C.; Li, C.; Choi, P. Y. K.; Nandakumar, K.; Kostiuk, L. W. A Novel Method for Molecular Dynamics Simulation in the Isothermal-Isobaric Ensemble. *Mol. Phys.* **2011**, *109*, 191−202.
(82) Bepari, A. K.; Reza, H. M. Identification of a Novel Inhibitor of SARS-CoV-2 3CL-PRO through Virtual Screening and Molecular Dynamics Simulation. *PeerJ* **2021**, *9*, No. e11261.
(83) Berendsen, H. J. C.; Postma, J. P. M.; van Gunsteren, W. F.; DiNola, A.; Haak, J. R. Molecular Dynamics with Coupling to an External Bath. *J. Chem. Phys.* **1984**, *81*, 3684−3690.
(84) Parrinello, M.; Rahman, A. Polymorphic Transitions in Single Crystals: A New Molecular Dynamics Method. *J. Appl. Phys.* **1981**, *52*, 7182−7190.
(85) Kushwaha, P. P.; Singh, A. K.; Bansal, T.; Yadav, A.; Prajapati, K. S.; Shuaib, M.; Kumar, S. Identification of Natural Inhibitors Against SARS-CoV-2 Drugable Targets Using Molecular Docking, Molecular Dynamics Simulation, and MM-PBSA Approach. *Front. Cell. Infect. Microbiol.* **2021**, *11*, 730288.
(86) Jiang, Z.; You, L.; Dou, W.; Sun, T.; Xu, P. Effects of an Electric Field on the Conformational Transition of the Protein: A Molecular Dynamics Simulation Study. *Polymers* **2019**, *11*, 282.
(87) Afgan, E.; Baker, D.; Batut, B.; van den Beek, M.; Bouvier, D.; Čech, M.; Chilton, J.; Clements, D.; Coraor, N.; Grüning, B. A.; Guerler, A.; Hillman-Jackson, J.; Hiltemann, S.; Jalili, V.; Rasche, H.; Soranzo, N.; Goecks, J.; Taylor, J.; Nekrutenko, A.; Blankenberg, D. The Galaxy Platform for Accessible, Reproducible and Collaborative Biomedical Analyses: 2018 Update. *Nucleic Acids Res.* **2018**, *46*, W537−W544.
(88) Grant, B. J.; Rodrigues, A. P. C.; ElSawy, K. M.; McCammon, J. A.; Caves, L. S. D. Bio3d: An R Package for the Comparative Analysis of Protein Structures. *Bioinformatics* **2006**, *22*, 2695−2696.
(89) Wang, R. R.; Ma, Y.; Du, S.; Li, W. Y.; Sun, Y. Z.; Zhou, H.; Wang, R. L. Exploring the Reason for Increased Activity of SHP2 Caused by D61Y Mutation through Molecular Dynamics. *Comput. Biol. Chem.* **2019**, *78*, 133−143.
(90) Kumar, N.; Awasthi, A.; Kumari, A.; Sood, D.; Jain, P.; Singh, T.; Sharma, N.; Grover, A.; Chandra, R. Antitussive Noscapine and Antiviral Drug Conjugates as Arsenal against COVID-19: A Comprehensive Chemoinformatics Analysis. *J. Biomol. Struct. Dyn.* **2022**, *40*, 101−116.
(91) Wang, Z.; Wang, X.; Li, Y.; Lei, T.; Wang, E.; Li, D.; Kang, Y.; Zhu, F.; Hou, T. FarPPI: A Webserver for Accurate Prediction of Protein-Ligand Binding Structures for Small-Molecule PPI Inhibitors by MM/PB(GB)SA Methods. *Bioinformatics* **2019**, *35*, 1777−1779.
(92) Grasso, G.; di Gregorio, A.; Mavkov, B.; Piga, D.; Labate, G. F. D.; Danani, A.; Deriu, M. A. Fragmented Blind Docking: A Novel Protein−Ligand Binding Prediction Protocol. *J. Biomol. Struct. Dyn.* **2021**, 1−10.
(93) Yalçın, S.; Yalçınkaya, S.; Ercan, F. In Silico Detection of Inhibitor Potential of Passiflora Compounds against SARS-Cov-2(Covid-19) Main Protease by Using Molecular Docking and Dynamic Analyses. *J. Mol. Struct.* **2021**, *1240*, 130556.
(94) Bansod, S.; Raj, N.; R, A.; Nair, A. S.; Bhattacharyya, S. Molecular Docking and Molecular Dynamics Simulation Identify a

Novel Radicicol Derivative That Predicts Exclusive Binding to Plasmodium Falciparum Topoisomerase VIB. *J. Biomol. Struct. Dyn.* **2022**, *40*, 6939−6951.
(95) Venkateshan, M.; Muthu, M.; Suresh, J.; Ranjith Kumar, R. Azafluorene Derivatives as Inhibitors of SARS CoV-2 RdRp: Synthesis, Physicochemical, Quantum Chemical, Modeling and Molecular Docking Analysis. *J. Mol. Struct.* **2020**, *1220*, 128741.
(96) Mohapatra, R. K.; Azam, M.; Mohapatra, P. K.; Sarangi, A. K.; Abdalla, M.; Perekhoda, L.; Yadav, O.; Al-Resayes, S. I.; Jong-Doo, K.; Dhama, K.; Ansari, A.; Seidel, V.; Verma, S.; Raval, M. K. Computational Studies on Potential New Anti-Covid-19 Agents with a Multi-Target Mode of Action. *J. King Saud Univ., Sci.* **2022**, *34*, 102086.
(97) Li, L.; Li, C.; Sarkar, S.; Zhang, J.; Witham, S.; Zhang, Z.; Wang, L.; Smith, N.; Petukh, M.; Alexov, E. DelPhi: A Comprehensive Suite for DelPhi Software and Associated Resources. *BMC Biophys.* **2012**, *5*, 1−11.

https://doi.org/10.1021/acsomega.2c04837
ACS Omega 2023, 8, 391−409